Journal of Medicinal Chemistry

pubs.acs.org/jmc

Article

Discovery of AVI-6451, a Potent and Selective Inhibitor of the SARS-CoV-2 ADP-Ribosylhydrolase Mac1 with Oral Efficacy In Vivo

Priyadarshini Jaishankar,[⊥] Galen J. Correy,[⊥] Yusuke Matsui,[⊥] Takaya Togo,[⊥] Moira M. Rachman, Maisie G.V. Stevens, Eric R. Hantz, Jeffrey Zheng, Morgan E. Diolaiti, Mauricio Montano, Taha Y. Taha, Julia Rosecrans, Julius Pampel, Nevan J. Krogan, Brian K. Shoichet, Alan Ashworth, Melanie Ott, James S. Fraser,* and Adam R. Renslo*

Cite This: https://doi.org/10.1021/acs.jmedchem.5c02933

Read Online

ACCESS | Metrics & More | Article Recommendations | Supporting Information

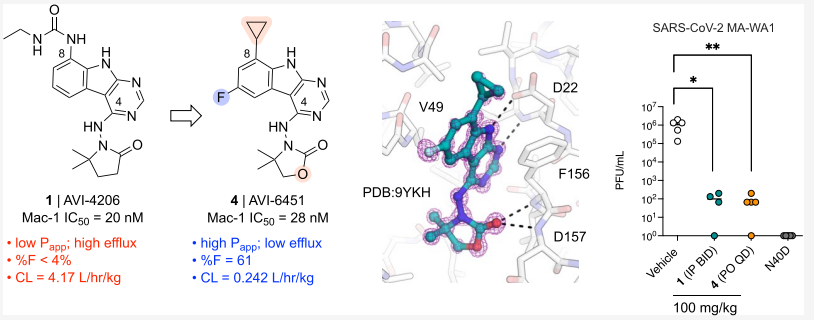

ABSTRACT: The COVID-19 pandemic emphasized the need for effective antivirals acting at new targets. We recently described AVI-4206, a 9*H*-pyrimido[4,5-*b*]indole-based inhibitor of the SARS-CoV-2 macrodomain Mac1, an ADP-ribosylhydrolase thought to blunt the host immune response to viral infection. While AVI-4206 represents the first Mac1 inhibitor to demonstrate in vivo efficacy in mouse infection models, its low oral bioavailability necessitated IP administration. Herein, we describe an extensive medicinal chemistry campaign to identify new leads with improved cellular permeability and high oral bioavailability. Various tactics were employed toward these ends, including an exploration of urea isosteres to reduce hydrogen bond donor count and total polar surface area. These efforts ultimately produced AVI-6451, a potent Mac1 inhibitor with low intrinsic clearance and high oral bioavailability that achieves superior antiviral efficacy with once-daily oral administration in a mouse model of SARS-CoV-2 infection.

INTRODUCTION

The COVID pandemic emphasized the urgent need for effective antiviral agents acting by novel mechanisms.[1,2] The SARS-CoV-2 macrodomain Mac1, part of the nonstructural protein 3 (NSP3), has emerged as an intriguing and novel target for the development of new antiviral agents.[3] Much of this enthusiasm derives from compelling genetic studies in which SARS-CoV-2 virus bearing deletion or inactivating mutations in Mac1 are found to have dramatically reduced pathogenesis in mice.[4,5] As an ADP-ribosylhydrolase, the function of Mac1 is to blunt the host immune response by removing ADP-ribose marks installed by host PARPs to mediate interferon signaling.[6,7] The discovery of Mac1 inhibitors has been pursued by our combined research groups and several others since the beginning of the COVID-19 pandemic.[7−11] Nevertheless, the identification of potent inhibitors with drug-like properties suitable for in vivo proof of concept studies had remained elusive. Recently, we reported the development of AVI-4206 (**1**), a potent Mac1 lead (IC_{50} = 20 nM) with an ADME and PK profile suitable for in vivo studies when administered by the intraperitoneal (IP) route.[12] Gratifyingly, in a lethal infection model involving K18-hACE2 mice infected with the WA1 strain of SARS-CoV-2, IP dosing of **1** at 100 mg/kg BID for 5 days produced both a survival benefit and significantly reduced viral titers in lung, thus providing the first pharmacological validation of Mac1 as an antiviral drug target.

Although its potency and selectivity profile make **1** a vital in vivo tool compound, its poor permeability and a high efflux in Caco2 assays unsurprisingly translated to limited (<5%) oral bioavailability in mouse. We attributed this to a surplus of hydrogen bond donors, including two in the C8 urea function

Received: October 10, 2025
Revised: December 1, 2025
Accepted: December 5, 2025

that engages Asp22 of Mac1. Empirical SAR led us to suspect the urea function as also contributing to P-gp recognition. In a search for alternate Mac1 lead chemotypes, we employed shape-based screening (FrankenROCS) using fused fragments as queries, to efficiently search across billions of tangible fragment- and lead-sized molecules.[13] Among the most promising fragments from this effort was the deazapurine (7*H*-pyrrolo[2,3-*d*]pyrimidine) analog **2** (AVI-1504, Figure 1), which exhibited excellent Caco2 permeability without efflux, combined with good ADME properties, and high ligand efficiency (L.E. = 0.43).

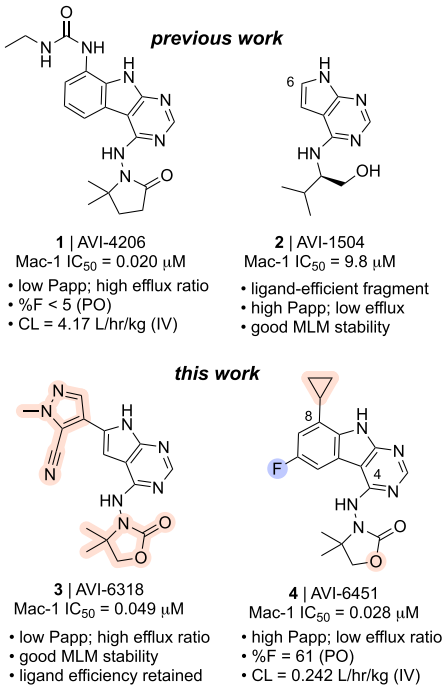

Figure 1. Structures and properties (top) of Mac1 inhibitor AVI-4206 (**1**) and a ligand-efficient deazapurine fragment AVI-1504 (**2**), described by our groups previously. Structures and properties (bottom) of optimized leads **3** (AVI-6318) and **4** (AVI-6451), the discovery of which is detailed herein.

As detailed herein, starting from these two distinct chemical starting points (i.e., **1** and **2**), we sought to develop potent, selective, and orally bioavailable Mac1 inhibitor leads that might more readily be applied in diverse PD studies, including in combination with other, approved oral agents. On the one hand, we describe the chemical evolution of fragment **2** to the potent ligand efficient lead **3** (AVI-6318; L.E. = 0.39, LipE = 6.0), by combining a heterocyclic urea surrogate at C6 with the introduction of an optimized oxazolidinone side chain at C4 (Figure 1). While successful in many aspects, the heterocyclic urea isostere approach leading to **3** failed to address the P-gp liability and did not yield meaningful improvements in PK profile.

A more successful effort was focused on **1** itself, and included a systematic exploration of C4 and C8 positions of the tricyclic core. This effort ultimately produced the potent (Mac1 IC_{50} = 28 nM) and orally bioavailable (61%F) lead AVI-6451 (**4**). In mouse, compound **4** achieves free plasma exposure above its Mac1 IC_{50} for a full 24 h after a single 50 mg/kg PO dose. The combination of low clearance and potent Mac1 inhibition produced superior oral efficacy in SARS-CoV-2 infected mice with once-daily administration at roughly half the total dose required with **1** via the IP route. Thus, the studies outlined herein provide both a case-study in addressing a thorny ADME liability, and a promising new Mac1 inhibitor lead and in vivo tool compound for studies of macrodomains in the innate immune response to viral infection.

RESULTS AND DISCUSSION

The complex structures of **1** and ADP-ribose bound to Mac1 reveal the key polar and hydrophobic interactions formed by substrate and inhibitor in the Mac1 active site (Figure 2).

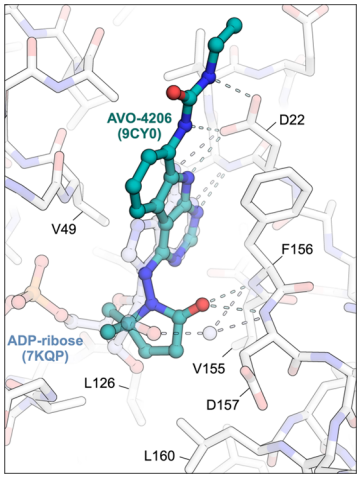

Figure 2. Superposition of the complex structures of **1** (9CY0) and ADP-ribose (7KQP) bound to Mac1 illustrating important polar contacts made with the backbone amides of F156/D157 in the ribose binding subsite and multiple hydrogen bonds with Asp22. Major hydrophobic contacts in the adenine site including side chains of F156, L126, L160, and V155 are indicated. A structured water mediates hydrogen bonding between ADP-ribose substrate and backbone amides of F156 and D157 in the ribose binding site.

These include aromatic (F156) and aliphatic (L126) amino acid side chains that flank the adenine and pyrimidoindole heterocycles, backbone amides (F156, D157), and hydrophobic side chains (V155, L160) in the 'southern' ribose binding site, and a 'northern' region comprising Asp22 that hydrogen bonds with the heteroaryl N−H and urea functions of substrate and inhibitor. Notably, polar interactions with the F156/D156 backbone is mediated by a water molecule in the case of ADP-ribose while the pyrrolidinone carbonyl of **1** forms direct hydrogen bonding contacts. A tunnel that leads to the catalytic machinery, and which binds the triphosphate of ADP-ribose is unoccupied by **1** and indeed yielded few hits in two prior fragment screening efforts.

In initial SAR studies leading to **1**, we found that an alkyl urea function at C8 formed productive H-bonding contacts with Asp22 and afforded ≥ 10-fold gains in potency as compared to C8 acetamide or carbamate functionality (Table 1). Of additional note is a hydrophobic cleft lying above and behind Asp22 (as viewed in Figure 2) that tolerates larger hydrophobes such as cyclopentane in the case of AVI-4057 (Mac1 IC_{50} = 42 nM). While aqueous solubility and mouse microsome stabilities of the urea analogs were favorable, efflux in Caco2 monolayers expressing P-gp was high (efflux ratio; ER > 10). At the C4 position, we found that introduction of gem-dimethyl substitution on the pyrrolidinone ring improved

https://doi.org/10.1021/acs.jmedchem.5c02933
J. Med. Chem. XXXX, XXX, XXX−XXX

Table 1. Structure–Activity Relationships in Early 9*H*-Pyrimidoindole Analogs Bearing C4 Pyrrolidinones Combined with C8 Urea or Related Side Chains[a]

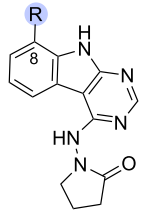

compound	R =
AVI-1499	NH_2
AVI-1501	NHAc
AVI-1500	NHC(=O)NHEt
AVI-3367	NHC(=O)OEt
AVI-3766	$NHSO_2NHMe$
AVI-4051	NHC(=O)NH-cyclopropyl
AVI-4057	NHC(=O)NH-cyclopentyl

compound	Mac1 IC_{50} (μM)	MLM $T_{1/2}$ (min)	Caco2 ER	K_{solb} (μM)
AVI-1499	0.63	>120		294
AVI-1501	1.6	>120	39.2	355
AVI-1500	0.083	>120	51.6	418
AVI-3367	3.1			
AVI-3766	2.0			
AVI-4051	0.19			
AVI-4057	0.042	>120	311	315

[a]Mac 1 IC_{50} in HTRF assay; MLM = mouse liver microsome stability; ER = efflux ratio; K_{solb} = kinetic solubility in pH 7.4 PBS. See Supplemental Figure S1 for dose–response curves.

potencies up to 5-fold across the series, but unfortunately did not mitigate high efflux in Caco2 assays.

Notably, the FrankenROCS fragment screening campaign[13] had identified several alternate C4 side chains for the 'southern' ribose binding site of Mac1, many of which could be applied beneficially in either the deazapurine (e.g., **2**) or tricyclic 9*H*-pyrimido[4,5-*b*]indole (e.g., **1**) series. In the complex structure of **2**, for example, the C4 valinol side chain formed hydrophobic and polar contacts that mimic, respectively, those of the gem-dimethyl and carbonyl functions of the pyrrolidinone C4 side chain in **1**. Being fragment-sized, **2** formed limited interactions with the northern site, apart from a hydrogen bond between in the indole-like N–H and Asp22. As noted, fragment **2** was of considerable interest given its promising ADME profile, which included high permeability ($P_{app\ A\text{-}B}$ = 14.9 × 10^{-6} cm/s) and lack of efflux (ER = 0.79) in Caco2 monolayers.

To improve the potency of **2** while maintaining its ADME profile we targeted Asp22 and the surrounding hydrophobic cleft that binds distal alkyl substituent of C8 urea analogs like **1** (Table 1). Tactically, this involved the exploration of C6 heterocycles that mimic an amide or urea function (i.e., with N–H or C–H donors) while also contacting the hydrophobic cleft (Chart 2 and Table 2). As an added benefit, modification of the C6 position in the deazapurine scaffold was much more tractable than analogous modification of the C8 position in **1**. Hence, in contrast to a ∼6–10 step synthesis required for **1** and its analogs, a streamlined 2–3 step synthetic route involving SNAr and Suzuki coupling reactions yielded the desired aryl and heteroaryl C6 deazapurine analogs (Scheme 1).

Scheme 1. Synthesis of Deazapurine Analogs Described Below in Chart 1 (Top Scheme) and Chart 2 (Bottom Scheme)[a]

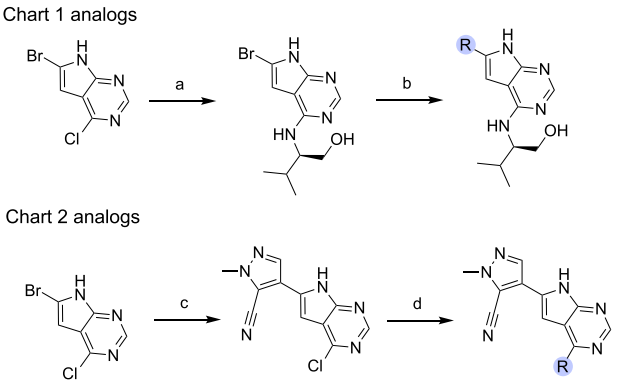

[a]Conditions: (a) (*R*)-2-amino-3-methylbutan-1-ol, Et_3N, DMSO, 110°C, 16 h, 45%. (b) R-$B(OH)_2$, $Pd(dppf)Cl_2$, Cs_2CO_3, dioxane-water (10:1), 110 °C, 10–60%; (c) 1-methyl-4-(pinacolborane)-1H-pyrazole-5-carbonitrile, dioxane-water (10:1), $Pd(dppf)Cl_2$, K_2CO_3, 95 °C, 2 h, 72%; (d) R-NH_2, iPrOH, aq. HCl, 100 °C, 10–65%.

More than 20 C6 (hetero)aryl analogs were prepared (Chart 1 and Table 2) and their complex structures revealed a conserved binding mode across the series (Figure 3). Aryl substitution at C6 was tolerated and generally produced a 2–4-fold improvement over **2** in Mac1 IC_{50} values, as determined in a homogeneous time-resolved fluorescence (HTRF) ligand displacement assay.[7] Analogs with electron withdrawing ortho substituents (F, CN) were moderately but consistently more potent than comparators (Cl, CH_3) possibly due to more favorable interaction of Asp 22 with the acidified ortho C–H bond of the aryl ring. This was supported by the complex structure of ortho-F analog AVI-4678 in which the flanking ortho C–H bond is directed toward Asp22 (Figure 3).

In addition to aryl C6 substituents, both 5- and 6-membered heterocycles were explored at C6, including ring systems capable of presenting either N–H, acidified C–H, or a heterocyclic S atom (σ-hole) for interaction with Asp22. We

Table 2. In Vitro ADME Data for AVI-1504 and Selected C6-Substituted Analogs from Chart 1[a]

compound	Mac1 HTRF IC_{50} (μM)	MLM CL (μL/min/mg)	MLM $T_{1/2}$ (min)	Caco2 Papp A to B ($\times10^{-6}$ cm/s)	Caco2 Papp B to A ($\times10^{-6}$ cm/s)	kinetic solubility in pH 7.4 PBS (μM)
AVI-1504 (2)	9.8	<11.6	>120	14.9	11.3	370
AVI-4678	1.9	611	2.3	17.4	13.2	479
AVI-4334	1.1	841	1.65	10.2	16.5	498
AVI-4684	0.27	354	3.92	2.12	16.7	476
AVI-4683	0.40	198	7.00	3.82	17.6	457
AVI-4266	0.77	29.1	47.6	0.2	15.3	508
AVI-4054	0.33	52.3	26.5	0.56	16.3	549

[a]Mac 1 IC_{50} in HTRF assay; MLM = mouse liver microsome clearance; Caco2 apparent permeability in apical to basolateral (A to B) and basolateral to apical (B to A) directions; kinetic solubility in pH 7.4 PBS. See Figure S1 for dose–response curves.

https://doi.org/10.1021/acs.jmedchem.5c02933
J. Med. Chem. XXXX, XXX, XXX–XXX

Chart 1. Structure, Mac1 Activity, and Selected ADME Data for Novel Analogs Bearing Aryl and Heteroaryl Substitutions at C6 of the 5-Deazapurine Ring[a]

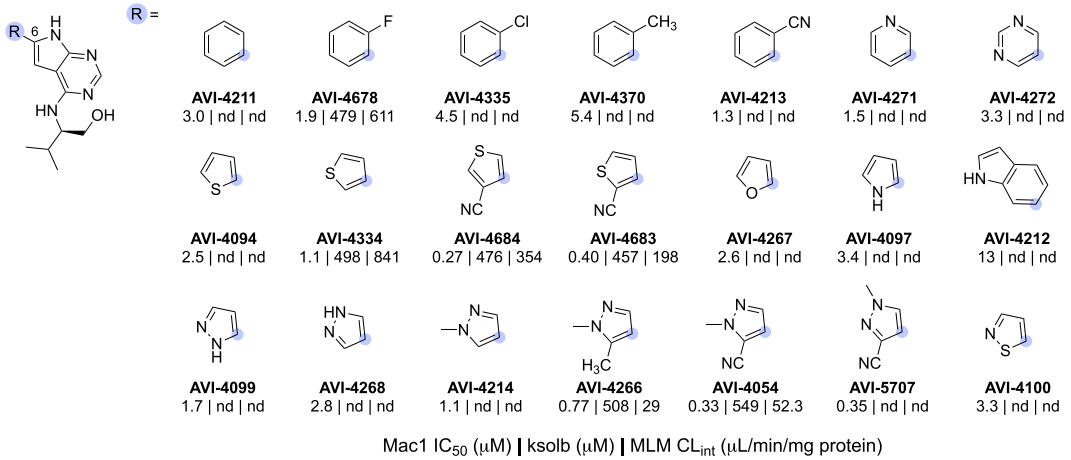

[a]Mac1 HTRF IC_{50}, kinetic solubility and mouse liver microsome clearance values are indicated below the AVI-ID. See Figure S1 for dose-response curves. nd: not determined.

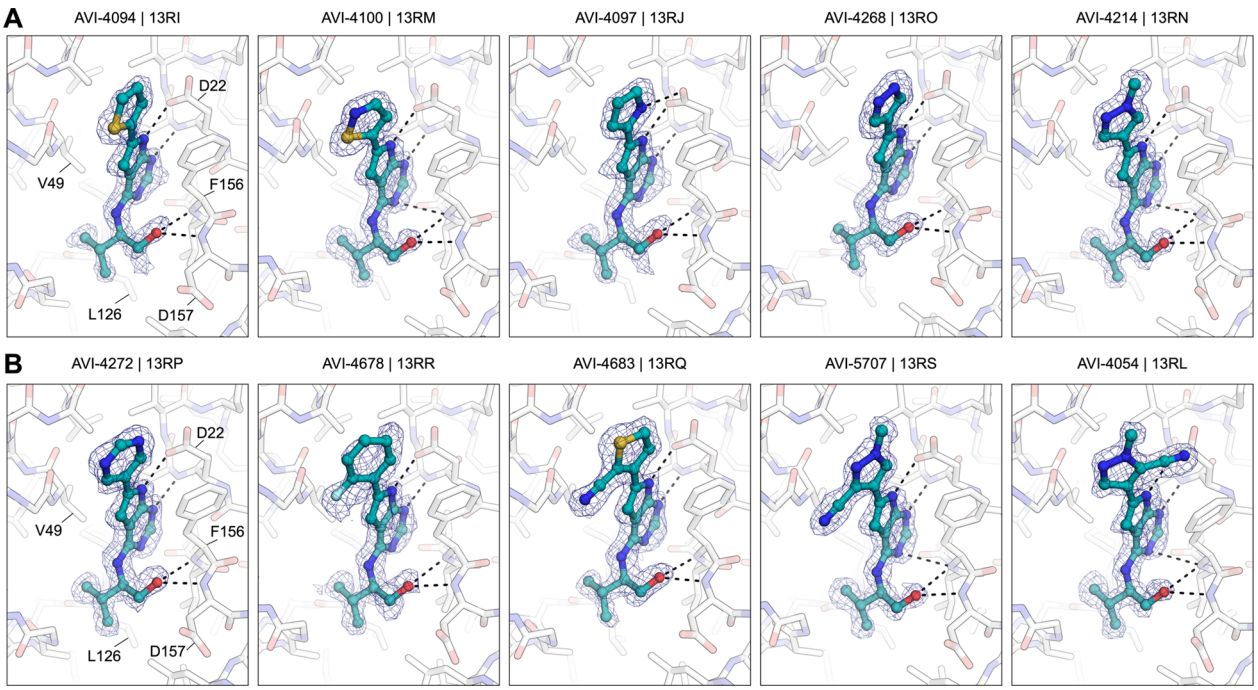

Figure 3. Complex structures of analogs from Chart 1 bound to Mac1. Panel (A) from left to right, AVI-4094, AVI-4100, AVI-4097, AVI-4268, AVI-4214. Panel (B) left to right, AVI-4272, AVI-4678, AVI-4683, AVI-5707, AVI-4054. PanDDA event maps are contoured around ligands at 2 σ (blue mesh). Hydrogen bonds are shown with dashed black lines.

found that pyridin-3-yl (AVI-4271), pyrimid-3-yl (AVI-4272), thiophen-2-yl (AVI-4094), thiophen-3-yl (AVI-4334), furan-2-yl (AVI-4267), pyrrol-2-yl (AVI-4097)), 1*H*-pyrazol-5-yl (AVI-4099), 1*H*-pyrazol-4-yl (AVI-4268), and isothiazol-5-yl (AVI-4100) analogs were either equipotent or modestly more potent than unsubstituted aryl comparator AVI-4211. This revealed broad tolerance for flat (hetero)aryl substitution at C6, but also suggested that these substituents did not form optimal polar interactions with Asp22. It was curious that analogs with an N−H donor (AVI-4099 and AVI-4097) or empty σ orbital (AVI-4100) positioned for contact with Asp22 were no more potent than those lacking such functionality. Indeed, while the pyrrole N−H of AVI-4097 did appear to interact with Asp22, the S atom of AVI-4100 was oriented away from Asp22 (Figure 3). From an ADME perspective, the introduction of aryl or thiophene rings at C6 notably led to reduced stability in liver microsomes, while good aqueous solubility was retained (Table 2). Caco2 permeability varied widely across the various (hetero)aryl C6 analogs, from high for C6 fluoroaryl (AVI-4678) to low for C6 pyrazoles generally (e.g., AVI-4266).

Since an ortho withdrawing group (F or CN) had proven beneficial in the aryl series, we next explored analogous substitution in the heteroarene series. Gratifyingly, an ortho CN afforded enhanced potencies in both thiophen-3-yl analogs (AVI-4683 and AVI-4684) and pyrazol-4-yl analogs (AVI-4054 and AVI-5707), with Mac1 IC_{50} values improved ∼3−4-fold

https://doi.org/10.1021/acs.jmedchem.5c02933
J. Med. Chem. XXXX, XXX, XXX−XXX

Chart 2. Novel Analogs Bearing Cyanopyrazole Substitution at C6 and Diverse Substitutions at C4 of the 5-Deazapurine Ring[a]

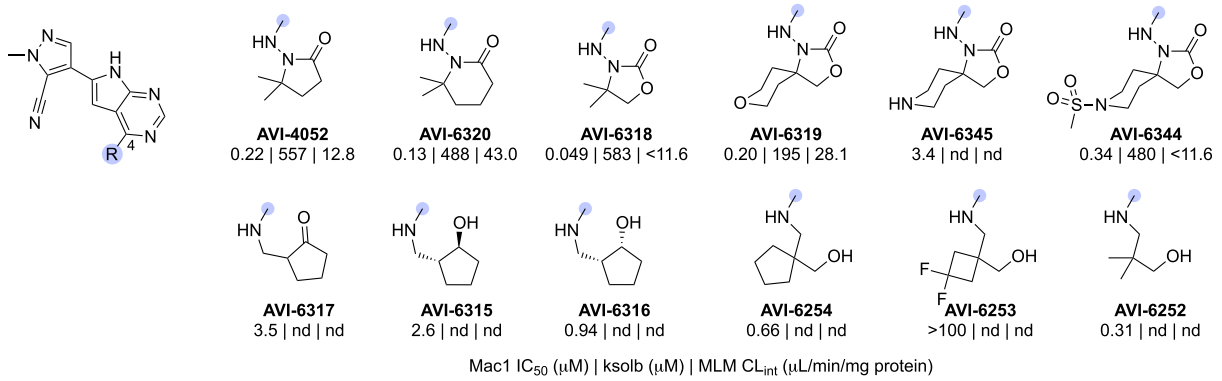

[a]Mac1 HTRF IC_{50}, kinetic solubility and mouse liver microsome clearance values are indicated below the AVI-ID. See Figure S1 for dose-response curves.

Table 3. In Vitro ADME Data for AVI-4054 and Selected Additional C4-Substituted Analogs from Chart 2[a]

compound	Mac1 HTRF IC_{50} (μM)	MLM CL (μL/min/mg)	MLM $T_{1/2}$ (min)	Caco2 Papp A to B ($\times 10^{-6}$ cm/s)	Caco2 Papp B to A ($\times 10^{-6}$ cm/s)	kinetic solubility in pH 7.4 PBS (μM)
AVI-4054	0.33	52.3	26.5	0.56	16.3	549
AVI-4052	0.22	12.8	108	0.158	11.7	557
AVI-6320	0.13	43.0	32.2	0.66	21.1	488
AVI-6318	0.049	<11.6	>120	0.138	13.5	583
AVI-6319	0.20	28.1	49.3	0.049	4.36	195
AVI-6344	0.34	<11.6	>120	0.072	0.52	480
AVI-6252	0.31	67.0	20.7	2.0	18.7	8.4

[a]Mac 1 IC_{50} in HTRF assay; MLM = mouse liver microsome clearance; Caco2 apparent permeability in apical to basolateral (A to B) and basolateral to apical (B to A) directions; kinetic solubility in pH 7.4 PBS. See Figure S1 for dose−response curves.

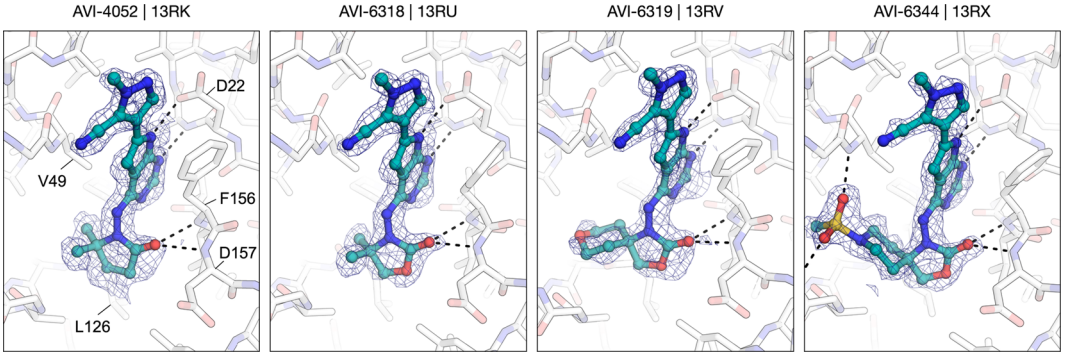

Figure 4. Complex structures of analogs from Chart 2 bound to Mac1. From left to right, AVI-4052, AVI-6318, AVI-6319, and AVI-6344. PanDDA event maps are contoured around ligands at 2 σ (blue mesh). Hydrogen bonds are shown with dashed black lines.

into the mid-nM regime (0.27−0.40 μM). The complex structures of C6 analogs showed an overall similar binding mode with a C−H bond preferentially oriented toward Asp22 (Figure 3). This suggests a weak C−H--O interaction with Asp22, where the effect of the CN is likely to polarize the C−H bond, producing a stronger H-bond donor. However, distinct orientations of the cyanopyrazole ring in complex structures of regioisomers AVI-4054 and AVI-5705 (Figure 3B) indicated that other factors, such as favorable disruption of water networks (i.e., entropic effects), might be as important as favorable enthalpic contact with Asp22, at least in the case of the C6 (hetero)aryl series of analogs.

In summary, a survey of C6 heteroaryl substituents yielded analogs up to ∼30-fold more potent than **2**, confirming the northern site as a fruitful one for driving potency. Conversely, the addition of C6 aryl or heteroaryl rings in **2** introduced metabolic instability in mouse liver microsomes and in many cases reduced Caco2 permeability and increased efflux (Table 2).

Expanding SAR around C6 cyanopyrazole analogs like AVI-4054, we explored diverse C4 side chains to better engage the ribose binding site and phosphate tunnel of Mac 1. Analogs of this type (Chart 2) were prepared by an analogous synthetic route wherein the shared cyanopyrazole C6 substituent was introduced by Suzuki coupling first, followed by SNAr reactions with amine-bearing C4 side chains (Scheme 1 and Supporting Information). The majority of C4 side chains were inspired by the gem-dimethylpyrrolidinone of **1**, (AVI-4052), such as the piperidin-2-one AVI-6320 and oxazolidinone AVI-6318, and analogs bearing spirocyclic tetrahydropyran (AVI-6319) or piperidine (AVI-6345 and AVI-6344) rings to engaged the phosphate tunnel (Chart 2, top row). Encourag-

https://doi.org/10.1021/acs.jmedchem.5c02933
J. Med. Chem. XXXX, XXX, XXX−XXX

ingly, these new analogs were generally 2−5-fold more potent that AVI-4054, while specific examples such as AVI-6318 (**3**) combined potent Mac1 inhibition (IC_{50} = 49 nM) with excellent solubility and mouse liver microsome stability (Table 3). The complex crystal structures of AVI-4052 and **3** revealed analogous binding modes with the C−H bond of the pyrazole ring oriented toward Asp22 and the carbonyl of the pyrrolidinone or oxazolidinone rings forming H-bonding contact with the backbone N−H groups of Phe156 and Asp157 (Figure 4). The ∼4-fold greater potency of oxazolidinone **3** vs pyrrolidinone AVI-4052 was notable, and reflected in a shorter hydrogen bond to the oxazolidinone carbonyl in its complex structure (Figure 4). While less potent than **3**, analogs AVI-6319 and AVI-6344 presented their spirocyclic rings toward the phosphate tunnel, as predicted. Notably, the piperidine sulfonamide function in AVI-6344 formed H-bonding contacts with the same backbone residues that H-bond to the α phosphate of ADP-ribose (cf. Figures 2 and 4). The binding mode of AVI-6344 hints at a potential for even more productive engagement of the phosphate tunnel in analogs of this C4 chemotype.

In terms of their ADME properties, oxazolidinone analogs **3**, AVI-6319, and AVI-6344 all showed notable improvements in microsome stability when compared to the progenitor lead AVI-4054. However, all four compounds exhibited Caco2 efflux ratios (ER ≥ 10) that were much higher than the early deazapurine lead **2**. In a final attempt to divorce P-gp recognition from the C6 heterocyclic deazapurines, we introduced a collection of more novel C4 side chains, some taken from, or inspired by, the FrankenROCS based screening effort. These included small to medium ring hydrophobes bearing carbonyl or hydroxyl functions to engage the backbone amides of the ribose binding site (Chart 2, bottom row). The most potent of these analogs was the acyclic analog AVI-6252, which retained the potency of pyrrolidinone AVI-4052, but at the expense of reduced metabolic stability and aqueous solubility, and without meaningful improvements to efflux (ER ∼ 9).

An early PK study of AVI-4052 and **1** (10 mg/kg IP) revealed a remarkably similar plasma exposure profile (Figure 5) consistent with their similar ADME profiles and plasma protein binding values (61 and 72%, respectively) and despite their distinct chemical scaffolds. The PK data suggested that a 100 mg/kg IP dose of AVI-4052 would be sufficient to maintain a free plasma exposure above its Mac1 IC_{50} values for several hours (blue dotted line, Figure 5). Although more potent deazapurine analogs, such as **3**, were ultimately identified, their overall similar ADME profiles, and remaining high efflux ratios, discouraged further evaluation of deazapurine analogs in vivo. Accordingly, the focus returned to **1** and the original 9*H*-pyrimido[4,5-*b*]indole scaffold.

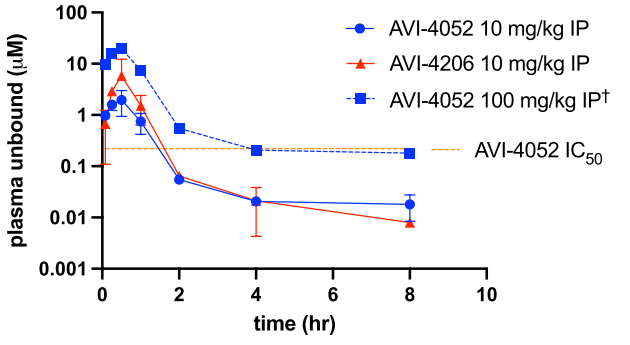

Figure 5. Unbound plasma exposure of **1** (AVI-4206) and AVI-4052 following a single IP dose of 10 mg/kg in mice. †Extrapolation of the free plasma exposure of AVI-4052 to a 10-fold higher dose, assuming linear pharmacokinetics. The Mac1 IC_{50} value of AVI-4052 is shown as an orange dotted line.

Initial SAR leading to **1** showed that even large alkyl ureas were well tolerated as C8 substituents (e.g., cyclopentyl urea AVI-4057; Mac1 IC_{50} = 42 nM, Table 1). We considered whether further modification of the urea might abrogate recognition by P-gp. However, analogs with six-membered oxygen-bearing heterocycles (AVI-6188), or those with an extended acyclic methoxyethyl urea (AVI-6187) failed to notably reduce efflux, despite excellent potencies (IC_{50} ∼ 20 nM) and microsome clearance values (Table 4).

Table 4. Potency and In Vitro ADME Data for C8 Urea Isosteric Analogs Bearing Pyrrolidinone or Oxazolidinone at C4[a]

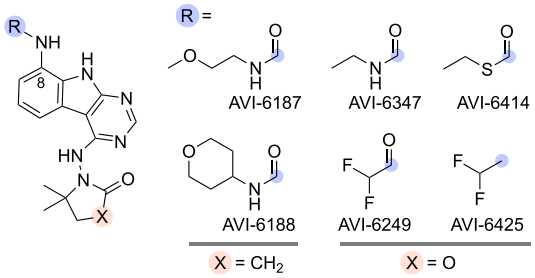

compound	Mac1 IC_{50} (μM)	MLM $T_{1/2}$ (min)	Caco2 ER	K_{solb} (μM)
AVI-4206	0.020	>120	241	505
AVI-6187	0.051	>120	54.9	468
AVI-6188	0.013	>120	71.5	542
AVI-6347	0.020	>120	100	498
AVI-6414	0.24	42	46.1	232
AVI-6249	0.45	73.1	102	518
AVI-6425	0.026	42.9	99.0	501

[a]Mac 1 IC_{50} in HTRF assay; MLM = mouse liver microsome stability; ER = efflux ratio BtoA/AtoB; Ksolb = kinetic solubility in pH 7.4 PBS. See Figure S1 for dose−response curves.

Next, we explored urea bioisosteres in which the distal N−H function of the urea was replaced by a sulfur atom as in thiocarbamate AVI-6414, or a polarized C−H bond as in difluoroacetamide AVI-6249 (Table 4). These analogs were prepared with the more optimal C4 oxazolidinone moiety, after we had first confirmed this modification of **1** afforded excellent potency, solubility, and MLM values (i.e., oxazolidinone AVI-6347). Unfortunately, both the ethyl thiocarbamate (AVI-6414) and difluoroacetamide (AVI-6249) analogs were ∼10-fold less potent, with still unacceptable efflux ratios and moderately reduced microsome stability (Table 4). Importantly, however, a difluoroethylaniline analog (AVI-6425) was equipotent to ethyl ureas **1** and AVI-6347, with an IC_{50} = 26 nM. While Caco2 ER remained high for AVI-6425, the excellent potency of this analog motivated an exploration of other small nonurea C8 substituents.

A pivotal set of such analogs included the C8 methyl, trifluoromethyl, and cyclopropyl analogs, prepared with either C4 pyrrolidinone or oxazolidinone side chains (Chart 3). Importantly, we found the C8 cyclopropyl analogs AVI-6354

https://doi.org/10.1021/acs.jmedchem.5c02933
J. Med. Chem. XXXX, XXX, XXX−XXX

Chart 3. Structure of 9*H*-Pyrimidoindole Leads Bearing Optimized C4 Heterocycles and Nonurea Substituents at C8[a]

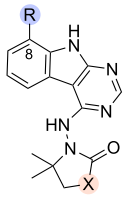

compound	X =	R =
AVI-6355	CH_2	Me
AVI-6371	CH_2	CF_3
AVI-6354	CH_2	cyclopropyl
AVI-6357	O	Me
AVI-6372	O	CF_3
AVI-6373	O	cyclopropyl

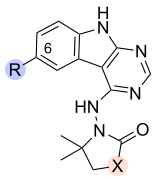

compound	X =	R =
AVI-3769	CH_2	CF_3
AVI-3865	CH_2	cyclopropyl
AVI-6412	O	CF_3

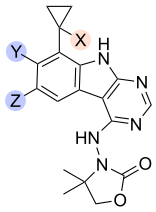

compound	X =	Y =	Z =
AVI-6451	H	H	F
AVI-6452	H	F	H
AVI-6612	OH	H	F
AVI-6613	F	H	F

[a]See Figure S1 for dose−response curves.

Table 5. Potency and In Vitro ADME Data for Compounds from Chart 3[a]

compound	Mac1 HTRF IC_{50} (μM)	MLM CL (μL/min/mg)	MLM $T_{1/2}$ (min)	Caco2 Papp A to B (x 10^{-6} cm/s)	Caco2 ER	mouse PPB (%)	K_{solb} (μM)
AVI-4206 (**1**)	0.022	<11.6	>120	0.023	241	61	505
AVI-6355	0.14	23.2	59.7				504
AVI-6371	1.3						
AVI-6354	0.11	17.2	80.4	13.6	1.3	87.6	485
AVI-6357	0.058−0.069	12.5	111	12.5	1.4	66.2	83.4
AVI-6372	1.3						
AVI-6373	0.085	12.9	108	10.8	1.7	82.9	130
AVI-3769	0.34	<11.6	>120	6.75	2.1	91.3	539
AVI-3865	0.32	48.0	28.9				544
AVI-6412	0.20						
AVI-6452	0.13	69.3	20.0				139
AVI-6451 (**4**)	0.028	<11.6; < 11.6[†]	>120; > 120[†]	4.7	2.9	91.4	32.0
AVI-6612	0.12	14.0	98.8	1.4	10.4		68.8
AVI-6613	0.37	<11.6	>120				3.0

[a]Mac 1 IC_{50} in HTRF assay; MLM CL = mouse liver microsome clearance; MLM $T_{1/2}$ = mouse liver microsome half-life; ER = efflux ratio = Caco2 $Papp_{B\ to\ A}/Papp_{A\ to\ B}$; PPB = plasma protein binding; Ksolb = kinetic solubility in pH 7.4 PBS. [†]Human liver microsome CL and $T_{1/2}$. See Figure S1 for dose−response curves.

Table 6. Selected PK Parameters for Mac1 Inhibitors Following a Single Dose in Male CD-1 Mice[a]

	IV 10 mg/kg				PO 50 mg/kg			
compound	CL (L/h/kg)	V_{ss} (L/kg)	AUC_{last} (hr*ng/mL)	MRT_{inf} (h)	C_{max} (ng/mL)	$T_{1/2}$ (h)	AUC_{last} (h*ng/mL)	F (%)
AVI-4206	4.17	1.32	2396	0.316	94	4.69	433	3.7
AVI-6451	0.242	1.07	41350	4.42	8863	3.91	124,756	61.0
AVI-6452	2.15	2.09	4645	0.97	4317	1.87	31,356	135

[a]PK parameters calculated based on total plasma exposure values. Studies performed in male CD-1 mice, with a formulation comprising 10% DMSO|50% PEG400|40% (20% hydroxypropyl-β-CD in water) at 2 mg/mL for IV arms and 5 mg/mL for PO arms. See Tables S1 and S2 and Figures S2 and S3 for full PK data.

and AVI-6373 to be ≥10-fold more potent than isosteric C8 trifluoromethyl analogs AVI-6371 and AVI-6372 (Table 5). This revealed a significant preference for more acidic C−H bonds, as in the cyclopropyl ring, over the inversely polarized C−F bonds of the CF_3 group. An alternate explanation involving electronic effects on the aryl π system could be ruled out by the observation that *C6-substituted* cyclopropyl (AVI-3865) and trifluoromethyl (AVI-3769) analogs showed almost identical IC_{50} values (Table 5 and Supporting Information Figure S1).

In summary, C8-cyclopropyl leads AVI-6354 and AVI-6373 exhibited potency approaching **1**, with two fewer hydrogen bond donors and calculated topological polar surface area (tPSA) reduced from 119 Å^2 to just 69 Å^2 (for AVI-6354). Strikingly, permeability in Caco2 monolayers was improved from 0.023 × 10^{-6} cm/s for **1** to 13.6 × 10^{-6} cm/s for AVI-6354, while ER plummeted from >200 to 1.3 (Table 5). The introduction of fluorine substitution at C6 or C7, yielded the key analogs AVI-6451 (**4**) and AVI-6452, respectively. Interestingly, C6 fluorination as in **4** returned a Mac1 IC_{50} = 28 nM, essentially equipotent to **1**, while C7 fluorination in AVI-6452 had the opposite effect on potency and also worsened microsome stability. Compound **4** demonstrated low clearance (<11.6 μL/min/mg) in both mouse and human liver microsomes and good Caco2 permeability with an acceptable efflux ratio of 2.9 (Table 5). Additional analogs of **4** in which the benzylic position was blocked with OH or F substitution were ∼ 5−10 fold less potent (AVI-6612 and AVI-6613).

The excellent potency and improved ADME properties of **4** led to its selection for mouse PK studies, where the compound exhibited remarkably low clearance (0.242 L/h/kg, ∼3% of liver blood flow), a favorable $T_{1/2}$ of ∼4 h, and a satisfying oral bioavailability value of 61%F (Table 6, Supplementary Figure S2 and Table S1A−C). By comparison, C7-F comparator AVI-6452 showed higher clearance, and shorter $T_{1/2}$ values that were consistent with its reduced microsome stability (Table 3, Supplementary Figure S3 and Table S2A−C).

https://doi.org/10.1021/acs.jmedchem.5c02933
J. Med. Chem. XXXX, XXX, XXX−XXX

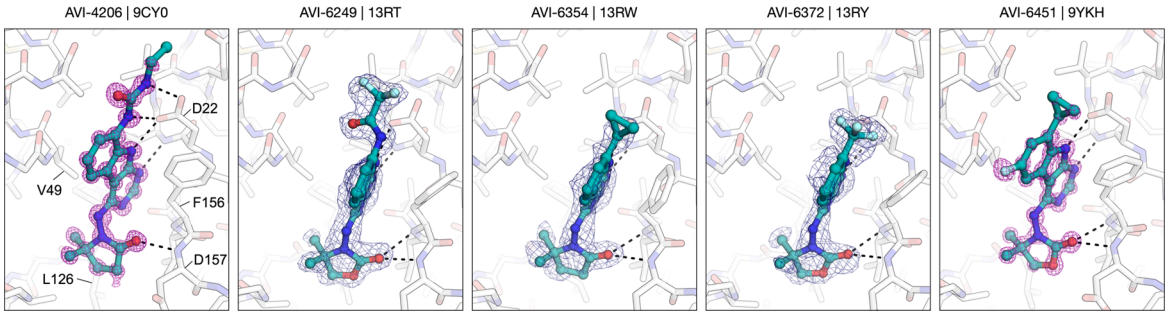

Figure 6. Complex structures of C8 urea and nonurea analogs bound to Mac1. From left to right, AVI-4206, AVI-6249, AVI-6354, AVI-6372, and AVI-6451 (**4**). PanDDA event maps are contoured around ligands at 2σ (blue mesh) and F_O-F_C difference electron density maps calcucalculated prior to ligand placement are contoured at 4σ (purple mesh). Hydrogen bonds are shown with dashed black lines.

The observation that a simple aliphatic C8 substituent in **4** could effectively replace the polar urea of **1** was a welcome, if surprising, finding. The complex structures of C8 cyclopropane and trifluoromethyl analogs AVI-6354 and AVI-6372 showed a nearly identical binding mode wherein Asp22 hydrogen bonds with the N−H function of the tricyclic core, with the carbonyl π surface of Asp22 in apparent contact with the C8 substituent (Figure 6). This predicts for more favorable electrostatic interaction with cyclopropane C−H bonds as compared to trifluoromethyl C−F bonds, consistent with the 10-fold difference in potency of these analogs. Notably, the orientation of Asp22 in the structure of **4** is similar to that of AVI-6354 and distinct from that of **1**, wherein the carboxylate turns to face and directly engage the urea N−H donors (Figure 6). Thus, the crystal structures of C8 urea, cyclopropyl, and trifluoromethyl analogs provided one possible rationale for the observed C8 SAR based on purely enthalpic grounds.

To gain additional insight, we turned to isothermal titration calorimetry (ITC) to experimentally determine enthalpic and entropic contributions to binding of analogs **1** and **4**. The potentially confounding effect of ring fluorination was examined by also assessing cyclopropyl analog AVI-6373, which lacks the C6 fluorination of **4**. While it is most common in ITC experiments to titrate ligand into protein, we found it necessary in this case to employ reverse titration of Mac1 protein into a solution of ligands, due to a significant heat of solvation observed in control experiments wherein **4** was added to the ITC buffer without Mac1. Having demonstrated no such complications with reverse addition of protein to ligand, we were able to measure the heat released upon binding and could record accurate thermodynamic parameters for all three compounds (Table 7).

Table 7. Thermodynamic Parameters of Mac1 Binding as Determined by ITC of Three Analogs

compound	K_d (nM)	ΔH (kJ/mol)	ΔS (J/K•mol)
AVI-4206 (**1**)	44 ± 18	−14.02 ± 0.41	94.6 ± 4.3
AVI-6451 (**4**)	55 ± 11	−27.00 ± 0.92	48.5 ± 3.7
AVI-6373	83 ± 10	−24.29 ± 0.65	54.0 ± 3.5

We found that ITC-determined K_d values for **1** and **4** were comparable within the standard error of the measurement (44 ± 18 and 55 ± 11 nM, respectively), and in reasonable agreement with their Mac1 IC_{50} values from the HTRF assay. The favorable effect of the C6−F substituent was confirmed by ITC, with a ∼2-fold improvement in the measured K_d for **4** vs AVI-6373. The contributions of ΔH and ΔS to their respective K_d values were similar, indicating that ring fluorination did not inordinately affect the thermodynamics of binding.

Returning to the comparison of **1** and **4**, we found that both had favorable ΔH and ΔS values, but the relative contributions of enthalpy and entropy were different. Thus, the urea **1** exhibited a smaller enthalpy of binding that was compensated for by a significantly greater increase in entropy, when compared to **4** (Table 7). This result was somewhat counterintuitive given that the urea−Asp22 interaction presumably involves precise positioning of interacting groups, and in isolation should be entropically costly. However, the preorganization of water networks in the apo vs bound state (i.e., desolvation of the ligands and binding site) must also be considered.

To gain further insight, density functional theory (DFT) was applied to calculate desolvation energies for compounds **1** and **4** using the wB97X-D/def2SVP//SMD(water)-wB97X-D/def2SVP level of theory (Table 8). The results indicated that

Table 8. Calculated Thermodynamic Parameters of Small Molecule Desolvation, Determined with DFT wB97X-D|def2SVP and SMD(Water)-wB97X-D|def2SVP Level of Theory

compound	ΔG (kJ/mol)	ΔH (kJ/mol)	$T\Delta S$ (kJ/mol)
AVI-4206 (**1**)	117.11	115.60	−1.51
AVI-6451 (**4**)	78.29	75.79	−2.51

desolvation of urea **1** is enthalpically much more costly than for **4**, presumably due strong solvent interactions with the polar urea function. This desolvation penalty is naturally overcome through favorable interactions with the Mac1 active site (including with Asp22) and via entropic gains from the release of water molecules to bulk solvent. Together the ITC and DFT data reveal that while binding of **1** and **4** to Mac 1 is downhill both enthalpically and entropically, the binding of **1** is driven more by the entropic term (and likely by desolvation of the active site), while binding of **4** is more enthalpically driven, likely with fewer net water molecules released to the bulk solvent.

While the move from C8 urea (**1**) to cyclopropane (**4**) proved beneficial with regard to Caco2 permeability and efflux, its more lipophilic nature raised the question of off-target engagement. Previously, in vitro screening of **1** at 10 μM across ∼300 kinases, proteases, and enzyme/receptors revealed a remarkably favorable off-target profile.[12] Here we present off-target binding data for **4** alongside the previous data for **1** (both at 10 μM) in the SafteyScreen44 panel of common off-

https://doi.org/10.1021/acs.jmedchem.5c02933
J. Med. Chem. XXXX, XXX, XXX−XXX

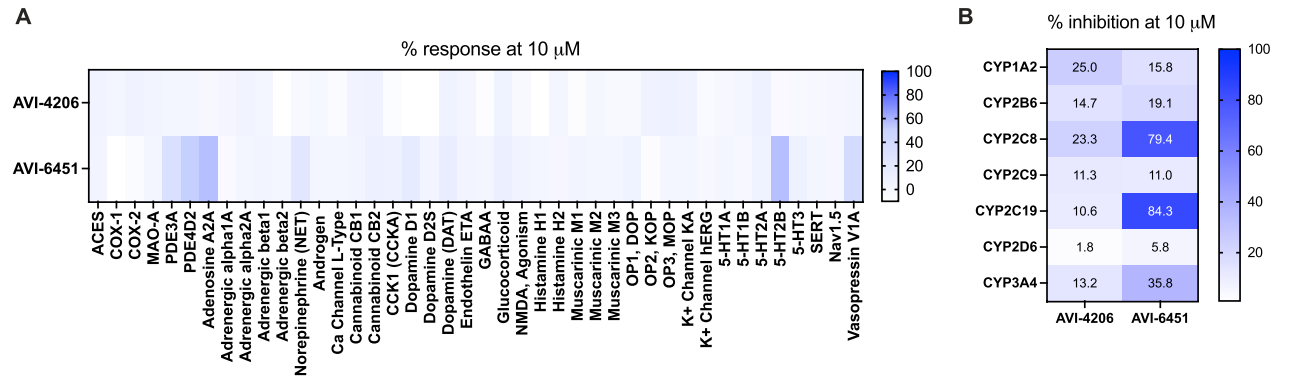

Figure 7. Heatmaps showing the activity of 10 μM AVI-4206 and AVI-6451 in (A) a Eurofins SafetyScreen 44 panel of potential enzyme and receptor off targets and (B) a panel of CYP isoforms.

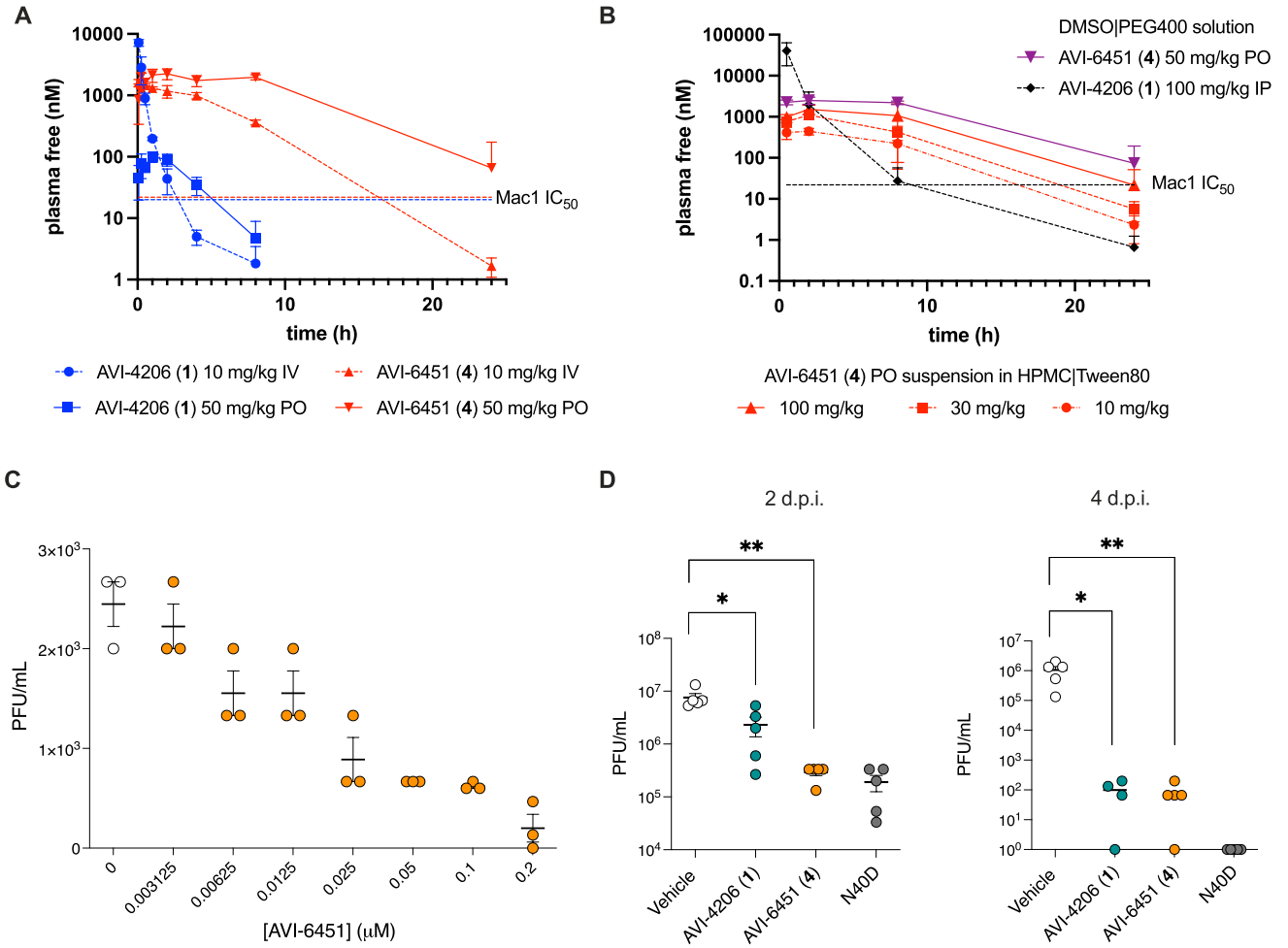

Figure 8. AVI-6451 shows enhanced PK and cellular and in vivo antiviral efficacy compared to AVI-4206. (A) Single-dose mouse PK experiments demonstrate the reduced clearance and higher oral exposure of AVI-6451 (**4**, in red) compared to AVI-4206 (**1**, in blue). Compounds formulated in 10% DMSO|50% PEG400|40% (20% HP-β-CD in water). (B) Dose escalation study of **4** formulated as a suspension in 1% (hydroxypropyl)methyl cellulose|1% Tween 80 in water. Data from prior studies with **1** and **4** in DMSO|PEG400|HP-β-CD are shown for comparison. (C) Dose-dependent antiviral activity of AVI-6451 (**4**, in orange) in monocyte derived macrophages infected with SARS-CoV-2 MA-WA1. (D) Viral load in the lungs of wild-type mice (N = 10/group) at days 2 and 4 postinfection with 1×10^4 PFU of SARS-CoV-2 MA-WA1. Mice were treated from day −1 to day 3 with vehicle, with 100 mg/kg AVI-4206 IP BID, or 100 mg/kg AVI-6451 PO QD. Viral load of mice infected with SARS CoV-2 MA-WA1 Mac1 N40D (mutant lacking Mac1 activity) are shown for comparison.

targets (Eurofins Panlabs, Inc.). Reassuringly, compound **4** showed a ≥50% response for only three of the off-targets in the panel, namely phosphodiesterase PDE4D2 (51%), the adenosine A_{2A} receptor (56%) and the serotonin 5-HT_{2B} receptor (56%) while retaining a favorable safety profile that was overall similar to **1** (Figure 7A). Against a panel of CYP enzymes, compound **4** at 10 μM showed more potent inhibition of CYP2C8 and CYP2C19 when compared to **1**,

https://doi.org/10.1021/acs.jmedchem.5c02933
J. Med. Chem. XXXX, XXX, XXX−XXX

identifying an area for further improvement in the optimization of this lead (Figure 7B).

Having identified **4** to be a potent, permeable, and orally bioavailable Mac1 inhibitor we were eager to explore its antiviral effects in cells and animals (Figure 8). As we and others have noted, the antiviral effects of Mac1 inhibitors is highly dependent on the cell model, with human airway organoid (HAO) and monocyte-derived macrophage (MDM) models showing the strongest Mac1 phenotype in our program.[12] Here we employed the MDM model to demonstrate superior cellular potency of **4**, compared to **1**, which was consistent with its higher cellular permeability in Caco2 assays. Thus, SARS-CoV-2 infection experiments were performed using MDM cells differentiated from CD14-positive monocytes isolated from human peripheral blood mononuclear cells (PBMCs). In these experiments, the presence of infectious viral particles is evaluated by plaque assay using Vero-TMPRSS2 cells. We found that both **1** and **4** exhibited antiviral effects in MDMs, but whereas **1** required μM concentrations to show antiviral effects in both the HAO and MDM models,[12] compound **4** was effective at mid to low nM concentrations (Figure 8C).

The superior oral PK profile of **4** results in >100-fold higher plasma exposure than **1** following a single oral dose (Table 6, Figure 8A). The free unbound plasma concentration of **4** remained well above its Mac1 IC_{50} a full 24 h after a 50 mg/kg oral dose, suggesting the potential for once-daily oral administration. To select dosing levels for PO administration in animal models, a dose-escalation PK study was performed with **4** using an oral suspension comprising 1% (hydroxypropyl)methyl cellulose and 1% Tween 80 in water. At the highest 100 mg/kg oral dose in this formulation, free plasma concentrations remained above Mac1 IC_{50} values for nearly 24 h and the compound was well tolerated (Figure 8B). On this basis, we selected once-daily oral administration of **4** at 100 mg/kg for evaluation in a SARS-CoV-2 infection model using the mouse-adapted MA-WA1 strain in wild type mice. A separate group of wild-type mice were infected with SARS-CoV-2 MA-WA1 Mac1 N40D, a mutant virus that lacks Mac1 enzymatic activity. As a positive control, we chose **1** at 100 mg/kg BID by the IP route as this dose had previously proven effective in multiple in vivo studies using a lethal mouse model using K18-hACE2 mice. Of note, while the K18-hACE2 is useful for demonstrating survival benefit, lethality in this model derives from viral invasion of the CNS, rather than pulmonary disease. Accordingly, it is generally regarded as a less than faithful model of clinical disease. Here therefore, we prioritized the use of wild-type mice and a mouse-adapted viral strain (MA-WA1) that better models the progression of lung pathology in human disease. Furthermore, this model is likely more relevant to intervention with a Mac1 inhibitor, where efficacy presumably derives from the restored ability of the immune system to clear the infection, once the brake conferred by Mac1 activity is released.

In the experiment, wild-type mice (N = 10 per group) were infected with 1×10^4 PFU of SARS-CoV-2 mouse-adapted (MA-WA1) strain and treated from day −1 to day 3 with either vehicle, compound **1** BID at 100 mg/kg via the IP route (DMSO|PEG|HP-βCD formulation) or with compound **4** as an oral suspension at 100 mg/kg QD via oral gavage. Viral load in lungs was assessed at 2 and 4 days postinfection (dpi) by plaque assay. Consistent with our prior studies of **1** in the K18-hACE2 mouse model, **1**-treated mice showed significantly reduced viral titers in lung compared to vehicle controls at 2 dpi and more dramatically at 4 dpi (Figure 8D). Notably, at roughly half the total dose (QD vs BID), and with PO rather than IP administration, compound **4** demonstrated a more significant reduction in viral load at 2 dpi compared to **1**-treated mice, and an excellent ∼4-log reduction in viral titers by 4 dpi. Also of note, the effect of once-daily PO administration of **4** in this model was comparable at 2 dpi to infection with the N40D Mac1 mutant virus, the first time we have observed small molecule inhibition of Mac1 to equal the pharmacodynamic effect of the N40D Mac1 mutant control bearing an inactivated Mac1 allele.

CONCLUSIONS

In summary, two chemical series were investigated in an effort to discover what is, to our knowledge, the first orally bioavailable and efficacious inhibitor of the SARS-CoV-2 ribosylhydrolase Mac1. As an improved in vivo tool compound and drug lead, compound **4** presents several advantages over **1** with regard to future studies of macrodomains as antiviral drug targets. These include suitability for once-daily oral administration in mice and a rapid antiviral effect that is evident at 2 dpi. These properties will enable shorter and more convenient dosing regimens when using **4** for pharmacodynamic studies, whether as a single-agent or in combination with other clinical or preclinical antivirals, and potentially in diverse coronavirus infection models. Moreover, the improved cellular permeability and potent antiviral effects of **4** revealed in the monocyte-derived macrophage assay nominate this compound for further cellular studies aimed an untangling the role of Mac1 in the innate immune response to viral infection, an area of active inquiry. With regard to the potential development of antiviral drug candidates from this scaffold, efforts are well underway and will be reported in due course.

EXPERIMENTAL PROCEDURES

Homogenous Time-Resolved Fluorescence (HTRF) Assay of Mac1 Inhibition. Binding of AVI analogs to Mac1 was assessed by the displacement of an ADPr conjugated biotin peptide from His6-tagged protein using an HTRF-technology based screening assay Mac1 protein expressed and purified as previously described.[12,14] Compounds were dispensed into ProxiPlate-384 Plus (PerkinElmer) assay plates using an Echo 650 Liquid Handler (Beckman Coulter). Binding assays were conducted in a final volume of 16 μL with 12.5 nM NSP3Mac1 protein, 200 nM peptide ARTK(Bio)QTARK(Aoa-RADP)S (Cambridge Peptides), 1:20000 Anti-His6-Eu^{3+} cryptate (HTRF donor, PerkinElmer AD0402) and 1:500 Streptavidin-XL665 (HTRF acceptor, PerkinElmer 610SAXLB) in assay buffer (25 mM 4-(2-hydroxyethyl)-1-piperazine-1-ethanesulfonic acid (HEPES) pH 7.0, 20 mM NaCl, 0.05% bovine serum albumin and 0.05% Tween-20). Assay reagents were dispensed manually into plates using an electronic multichannel pipet. Mac1 protein and peptide were dispensed and preincubated for 30 min at room temperature before HTRF reagents were added. Fluorescence was measured following a 1-h incubation at room temperature using a PerkinElmer EnVision 2105-0010 Dual Detector Multimode microplate reader with dual emission protocol (A = excitation of 320 nm, emission of 665 nm, and B = excitation of 320 nm, emission of 620 nm). Compounds were tested in triplicate in a 14-point dose response. Raw data were processed to give an HTRF ratio (channel A/B × 10,000), which was used to generate IC_{50} curves. The IC_{50} values were determined by nonlinear regression using GraphPad Prism v.10.0.2 (GraphPad Software, CA, USA). Data presented as mean ± SD of three technical replicates.

Macrophage Infection Assay. Macrophages were generated by culturing monocyte fractions isolated from peripheral blood

https://doi.org/10.1021/acs.jmedchem.5c02933
J. Med. Chem. XXXX, XXX, XXX−XXX

mononuclear cells (PBMCs) (Vitalant, CA, USA) using CD14 negative selection (STEMCELL Technologies, Vancouver, Canada) in serum-free medium supplemented with 50 ng/mL M-CSF for 8 days. The resulting monocyte-derived macrophages (MDMs) were pretreated with specified concentrations of AVI-6451 in the presence of 10 ng/mL IFN-γ for 2 h, followed by infection with SARS-CoV-2 isolate USA-WA1/2020 at a multiplicity of infection (MOI) of 2 for 2 h. After viral exposure, cells were thoroughly washed three times with phosphate-buffered saline (PBS) to remove unbound virus. The cells were then maintained in medium containing the respective compounds and 10 ng/mL IFN-γ for an additional 18 h. Viral particle production was subsequently quantified by plaque assay. Data analysis was carried out using GraphPad Prism version 10.2.0 (GraphPad Software, CA, USA).

Pharmacokinetic Studies. Procedures and data for PK studies of AVI-4052 and AVI-4206 (**1**) were reported previously. Mouse pharmacokinetic studies of AVI-6451 (**4**) and AVI-6452 with IV (10 mg/kg) or PO (50 mg/kg) dosing (Table 6, Figure 8, and Supplementary Tables S1 and S2) were performed in male CD1 mice (n = 9 per group) with a formulation of 10% DMSO/50% PEG400/40% of a 20% HP-β-CD solution in water. Dose escalation studies with **4** (Figure 8C) were performed in CD1 mice (n = 3) with administration by oral gavage using a suspension formulation of 1% (hydroxypropyl)methyl cellulose/1% Tween 80 at 1, 3, or 10 mg/mL for the 10, 30, and 100 mg/kg dosing levels, respectively. Animals were restrained manually at designated time points and ca. 110 μL of blood (30 μL in dose-escalation study with fewer mice/samples) was taken into K_2EDTA tubes via facial vein. The blood samples were collected on ice and centrifuged (2000 g, 5 min) to obtain plasma samples within 15 min post sampling. Three blood samples were collected from each mouse; three samples were collected at each time point. Plasma samples (20 μL) were diluted into 200 μL acetonitrile with internal standard (glipizide, 60 ng/mL) were analyzed by LC-MS/MS (triple quad 6500+) and quantified by comparison with a standard curve (1.0−3000 ng/mL) generated from authentic analyte. Data was processed by Phoenix WinNonlin (version 8.3); samples below limit of quantitation were excluded in the PK parameters and mean concentration calculation.

Pharmacodynamic Study in Mice. Pharmacodynamic studies were conducted in accordance with institutional and national ethical guidelines. Experiments involving replication-competent viruses were carried out in certified biosafety level-3 (BSL-3) facilities, following approval from the Institutional Biosafety Committees of the University of California, San Francisco, and the Gladstone Institutes. All animal procedures (protocol AN203103−00E) were reviewed and approved by the Institutional Animal Care and Use Committees of both institutions and performed in strict compliance with the National Institutes of Health Guide for the Care and Use of Laboratory Animals. C57BL/6J wild-type mice were housed in the Gladstone Animal Facility. Mice aged 6−8 weeks were randomly assigned to experimental groups and transferred to the ABSL-3 facility at the Gladstone Institutes. Mouse-adapted (MA) SARS-CoV-2 strains, MA-SARS-CoV-2 (Spike: Q498Y/P499T) and MA-SARS-CoV-2 Mac1 N40D, were generated using pGLUE, as previously described.[15] Mice were infected intranasally with MA-SARS-CoV-2 (1×10^4 PFU in 40 μL) under anesthesia induced by intraperitoneal injection of ketamine (150 mg/kg) and xylazine (10 mg/kg), and assigned to the following treatment groups: vehicle (PO, once daily), AVI-4206 (100 mg/kg, IP, twice daily), or AVI-6451 (100 mg/kg, PO, once daily). AVI-4206 was formulated in with a formulation of 10% DMSO/50% PEG400/40% of a 20% HP-β-CD solution in water for IP injection while AVI-6451 was administered by oral gavage as a suspension in 1% (hydroxypropyl)methyl cellulose and 1%Tween 80. A control group was infected with MA-SARS-CoV-2 Mac1 N40D under identical conditions. Compound administration began 1 day prior to infection (day − 1) and continued through 3 days postinfection. Mice were euthanized at 2 and 4 days postinfection. Lungs were harvested and homogenized using a bead homogenizer (zirconium bead tubes prefilled). Viral titers in lung homogenates were quantified via plaque assay. VeroE6-ACE2-TMPRSS2 cells were seeded in 12-well plates and incubated overnight at 37 °C with 5% CO_2. Serial dilutions$^{10-1 \text{ to } 10-6}$ of lung homogenates were prepared in serum-free DMEM and added to the cells for 1 h to allow viral adsorption. After adsorption, cells were overlaid with 2.5% Avicel (DuPont) in complete DMEM and incubated for 72 h. The overlay was then removed, cells were fixed with 10% neutral-buffered formalin for 1 h, stained with crystal violet, and plaques were counted to determine plaque-forming units (PFU).

Isothermal Titration Calorimetry. All ITC titrations were performed on an Affinity ITC Low Volume instrument (TA Instruments, WatersTM). Reactions were performed at 25 °C in 20 mM HEPES (pH 7.5) and 150 mM NaCl. Titrations were performed with 25 μM of ligand in the sample cell and 300 μM Mac1 in the injection syringe using 20 injections of 2.5 μL each at 200-s intervals with a 300-s initial baseline and 200-s postinjection baseline. Data was analyzed using the NanoAnalyze software v4.0.2.0 (TA Instruments, WatersTM). Thermograms were integrated and the normalized binding enthalpies fitted to an independent binding model (4-variable nonlinear least-squares fit). Thermodynamic parameters were then reported as the average and standard deviation obtained through five independent titrations.

Crystallography. The $P4_3$ crystals of SARS-CoV-2 Mac1 were grown from a solution containing 28% PEG 3000 and 100 mM CHES pH 9.5 as described previously.[8,13] Ligands were soaked into crystals to a final concentration of 10 mM using acoustic dispensing with an Echo 650 liquid handler.[16] Crystals were vitrified in liquid nitrogen without additional cryoprotection and X-ray diffraction data were collected at beamline 8.3.1 of the Advanced Light Source (ALS) and beamlines 9-2 and 12-2 of the Stanford Synchrotron Radiation Lightsource (SSRL). Data were indexed, integrated and scaled with XDS[17] and merged with Aimless.[18] Data collection statistics are provided in Table S3. Because several ligands bound with relatively low occupancy (<50%), we modeled ligands using PanDDA[19] event maps as described previously[8,13] using coordinates and restraints generated with phenix.elbow.[20] Coordinates were refined as a multistate model with both apo and ligand-bound states using phenix.refine[21] as described previously.[8,13] As we previously reported for AVI-4206,[12] low nanomolar Mac1 ligands dissolved the $P4_3$ crystals, presumably because a crystal contact is displaced when ligands bind to the adenosine site of chain B. To obtain a higher occupancy structure of AVI-6451, we cocrystallized Mac1 using an alternative construct that crystallizes in $P2_1$ or C2.[22] The Mac1-AVI-6451 complex was prepared by incubating protein (30 mg/mL, 1.6 mM) and compound (3.2 mM from a 100 mM stock in DMSO) at room temperature for 5 min. Co-crystals were grown using sitting drop vapor diffusion with drops containing 200 nl protein:AVI-6451 and 200 nl reservoir solution (200 mM lithium acetate and 20% PEG 3350). Diffraction data were collected at ALS 8.3.1 and processed as described above. Phases were obtained by molecular replacement using Phaser[23] and chain A of 7KQO as the search model. The initial model was improved by cycles of model building with COOT[24] and refinement with phenix.refine. Data collection and refinement statistics for the Mac1:AVI-6451 complex are reported in Supplemtary Data set S1. Crystallographic coordinates and structure factor intensities have been deposited in the PDB with the following accessing codes: 13RI, 13RJ, 13RK, 13RL, 13RM, 13RN, 13RO, 13RP, 13RQ, 13RR, 13RS, 13RT, 13RU, 13RV, 13RW, 13RX, 13RY, and 9YKH. Authors will release the atomic coordinates upon article publication.

Computational Density Functional Theory (DFT) Calculations. All computations were performed using Gaussian16 (Revision C.01). Geometry optimizations, force constants, and subsequent vibrational frequencies for compounds AVI-4206 and AVI-6451 were performed using the wB97X-D functional[25] and def2SVP basis set.[26] Gas-phase calculations were carried out using this level of theory. Solvation effects in water (epsilon = 78.3553) were evaluated using the same level of theory in conjunction with the SMD implicit solvation model[27] (SMD(water)-wB97X-Dldef2SVP). All calculations were performed at the default temperature (298 K) and pressure (1 atm). The thermodynamic parameters were determined by the

https://doi.org/10.1021/acs.jmedchem.5c02933
J. Med. Chem. XXXX, XXX, XXX−XXX

difference in electron energy (EE) with the appropriate correction term between the gas phase and implicit solvent model systems (=EE + Thermal Free Energy correction, =EE + Thermal Enthalpy Correction, = Entropy). The desolvation terms were determined based on the following equations:

$$\Delta G_{desolv} = -\Delta G_{solv} = G_{gas} - G_{solv}$$

$$\Delta H_{desolv} = -\Delta H_{solv} = H_{gas} - H_{solv}$$

$$\Delta S_{desolv} = -\Delta S_{solv} = S_{gas} - S_{solv}$$

All calculations were performed utilizing 30 CPUs, made available through UCSF's Wynton HPC cluster.

ADME Assays. In vitro ADME assays were performed at Quintara Discovery (Hayward, CA) using their standard experimental procedures and controls. Additional detail is provided in the Supporting Information File.

Safety Panel. The SafetyScreen44 receptor and ion channel off-target screen was performed by Eurofins Panlabs, Inc. Additional detail is provided in the Supporting Information File.

General Synthetic. Unless otherwise noted all chemical reagents and solvents used are commercially available. Air and/or moisture sensitive reactions were carried out under an argon atmosphere in oven-dried glassware using anhydrous solvents from commercial suppliers. Solvent removal was accomplished with a rotary evaporator at ca. 10−50 Torr. Microwave reactions were carried out in a CEM Discover microwave reactor. Chromatography was carried out using Isolera Four or CombiFlash NextGen 300 flash chromatography system with SiliaSep silica gel cartridges from Silicycle. Reverse phase chromatography was carried out on either,[1] Waters 2535 Separation module with Waters 2998 Photodiode Array Detector. Separations were carried out on XBridge Preparative C18, 19 × 50 mm column at ambient temperature using a mobile phase of water−acetonitrile containing a constant 0.1% formic acid or[2] Gilson GX-281 instrument, separations using Xtimate Prep C18, 21.2 × 250 mm, 150 Å, 10 μm particle size column at ambient temperature using a mobile phase of acetonitrile−water with 10 mM ammonium bicarbonate. LC/MS data were acquired on either (1) Waters Acquity UPLC QDa mass spectrometer equipped with Quaternary Solvent Manager, Photodiode Array Detector and Evaporative Light Scattering Detector. Separations were carried out with Acquity UPLC BEH C18 1.7 μm, 2.1 × 50 mm column at 25 °C, using a mobile phase of water−acetonitrile containing a constant 0.1% formic acid or (2) Agilent 1200 Infinity LC with an Agilent 1956 single quadrupole MS using electrospray ionization: Column: SunFire C18 (4.6 × 50 mm, 3.5 μm), Mobile phase: H_2O (10 mmol NH_4HCO_3) (A)/CH_3CN (B) at 50 °C with Photodiode Array Detector. Chemical shifts are reported in δ units (ppm). NMR spectra were referenced relative to residual NMR solvent peaks. Coupling constants (*J*) are reported in hertz (Hz). NMR spectra were recorded either on Bruker 500 MHz or Bruker Avance III HD 400 MHz spectrometer. All final analogs assessed in biochemical, cellular, or animal experiments were judged to be of ≥95% purity by HPLC and ^{1}H NMR analysis (See Supporting Information for representative HPLC chromatograms for key analogs).

Synthesis of 1-((8-Amino-9H-pyrimido[4,5-b]indol-4-yl)amino)-pyrrolidin-2-one (AVI-1499). A mixture of 4-chloro-9H-pyrimido[4,5-*b*]indol-8-amine (28 mg, 0.13 mmol) and 1-aminopyrrolidin-2-one hydrochloride (35 mg, 0.26 mmol) in isopropanol/water (10:1, 1.1 mL) were heated to 100 oC for 18 h. The reaction mixture was filtered, the residue was washed with ethyl acetate and dried to obtain 28 mg (77%) of AVI-1499 as brown solid. ^{1}H NMR (DMSO-d6, 400 MHz) δ 12.99 (br s, 1H), 8.62 (s, 1H), 7.92 (br d, 1H, *J* = 7.5 Hz), 7.27 (t, 1H, *J* = 7.9 Hz), 7.05 (br d, 1H, *J* = 7.5 Hz), 3.70 (br t, 2H, *J* = 6.9 Hz), 2.44−2.53 (m, 2H), 2.20 (br t, 2H, *J* = 7.4 Hz). LCMS (ESI): *m*/*z*= 283 $(M+H)^+$.

Synthesis of N-(4-((2-Oxopyrrolidin-1-yl)amino)-9H-pyrimido-[4,5-b]indol-8-yl)acetamide (AVI-1501). To a solution of 1-((8-amino-9H-pyrimido[4,5-*b*]indol-4-yl)amino)pyrrolidin-2-one (15 mg, 0.053 mmol) and triethylamine (0.015 mL, 0.11 mmol) in THF (1 mL), was added acetyl chloride (0.004 mL, 0.056 mmol). After stirring at 65 °C for 3 h, the reaction mixture was purified by reverse phase chromatography (water/acetonitrile/0.1% formic acid) to obtain 9 mg (50%) **AVI-1501** formate, as a white solid. ^{1}H NMR (METHANOL-d_4, 400 MHz) δ 8.39 (s, 1H), 7.90 (d, 1H, *J* = 7.8 Hz), 7.45 (d, 1H, *J* = 7.8 Hz), 7.19−7.21 (m, 1H), 3.81−3.85 (m, 2H), 2.59−2.63 (m, 2H), 2.27−2.31 (m, 5H). LCMS (ESI): *m*/*z*= 325 $(M+H)^+$.

Synthesis of 1-Ethyl-3-(4-((2-oxopyrrolidin-1-yl)amino)-9H-pyrimido[4,5-b]indol-8-yl)urea Formic Acid Salt (AVI-1500). To a solution of 4-chloro-9H-pyrimido[4,5-*b*]indol-8-amine (50 mg, 0.23 mmol) and triethylamine (0.064 mL, 0.46 mmol) in THF (2 mL), was added ethyl isocyanate (0.018 mL, 0.23 mmol). After stirring at 65 °C for 18 h, the reaction mixture was filtered. The residue was washed with ethyl acetate and dried to obtain 50 mg of 1-(4-chloro-9H-pyrimido[4,5-*b*]indol-8-yl)-3-ethylurea as a white solid that was used in the next step without further purification. ^{1}H NMR (DMSO-d_6, 400 MHz) δ 12.39 (br s, 1H), 8.80 (s, 1H), 8.43 (s, 1H), 7.96 (d, 1H, *J* = 7.6 Hz), 7.72 (d, 1H, *J* = 7.8 Hz), 7.35 (t, 1H, *J* = 7.9 Hz), 6.38 (s, 1H), 3.18−3.21 (m, 2H), 1.12 (t, 3H, *J* = 7.2 Hz). LCMS (ESI): *m*/*z*= 290, 292 $(M+H)^+$.

A mixture of 1-(4-chloro-9H-pyrimido[4,5-*b*]indol-8-yl)-3-ethylurea (26 mg, 0.09 mmol) and 1-aminopyrrolidin-2-one hydrochloride (25 mg, 0.18 mmol) in isopropanol/water (10:1, 1.1 mL) were heated to 100 °C for 18 h. The reaction mixture was purified by reverse phase chromatography (water/acetonitrile/0.1% formic acid) to obtain 8 mg (20%) **AVI-1500** formate as a white solid. ^{1}H NMR (DMSO-d_6, 400 MHz) δ 11.75 (br s, 1H), 9.31 (s, 1H), 8.53 (s, 1H), 8.41 (s, 1H), 7.97 (d, 1H, *J* = 7.8 Hz), 7.63 (d, 1H, *J* = 7.8 Hz), 7.20 (t, 1H, *J* = 7.9 Hz), 6.37 (br s, 1H), 3.70 (t, 2H, *J* = 7.1 Hz), 3.17−3.20 (m, 2H), 2.39−2.41 (m, 2H), 2.12−2.16 (m, 2H), 1.09−1.13 (m, 3H). ^{13}C NMR (DMSO-d_6, 100 MHz) δ 173.5, 156.2, 155.9, 155.5, 155.0, 128.5, 125.5, 121.3, 120.3, 117.1, 116.7, 96.4, 48.4, 34.8, 28.9, 16.7, 15.9. LCMS (ESI): *m*/*z*= 354 $(M+H)^+$.

Synthesis of Ethyl (4-((2-Oxopyrrolidin-1-yl)amino)-9H-pyrimido[4,5-b]indol-8-yl)carbamate Formic Acid Salt (AVI-3367). To a solution of 1-((8-amino-9H-pyrimido[4,5-*b*]indol-4-yl)amino)-pyrrolidin-2-one (15 mg, 0.053 mmol) and triethylamine (0.015 mL, 0.11 mmol) in THF (1 mL), was added ethyl chloroformate (0.005 mL, 0.056 mmol). After stirring at 65 °C for 18 h, the reaction mixture was purified by reverse phase chromatography (water/acetonitrile/0.1% formic acid) to obtain 2.7 mg (13%) **AVI-3367** formate as tan solid. ^{1}H NMR (METHANOL-d_4, 400 MHz) δ 8.42 (s, 1H), 7.94 (d, 1H, *J* = 7.8 Hz), 7.59 (br s, 1H), 7.28 (t, 1H, *J* = 7.9 Hz), 4.1−4.26−4.30 (m, 2H), 3.84 (t, 2H, *J* = 7.1 Hz), 2.60 (t, 2H, *J* = 8.0 Hz), 2.30−2.33 (m, 2H), 1.36−1.39 (m, 3H). LCMS (ESI): *m*/*z*= 355 $(M+H)^+$.

Synthesis of Methyl (4-((2-Oxopyrrolidin-1-yl)amino)-9H-pyrimido[4,5-b]indol-8-yl)sulfonamide Formic Acid Salt (AVI-3766). To a solution of 1-((8-amino-9H-pyrimido[4,5-*b*]indol-4-yl)amino)pyrrolidin-2-one (10 mg, 0.035 mmol), DMAP (2.2 mg, 0.18 mmol) and triethylamine (0.010 mL, 0.071 mmol) in DMA (0.5 mL), was added methylsulfamoyl chloride (15 mg, 0.11 mmol). After stirring at 65 °C for 90 h, the reaction mixture was purified by reverse phase chromatography (water/acetonitrile/0.1% formic acid) to obtain 2.6 mg (17%) **AVI-3766** formate as brown solid. ^{1}H NMR (METHANOL-d_4, 400 MHz) δ 8.44 (s, 1H), 8.01 (d, 1H, *J* = 7.8 Hz), 7.51 (d, 1H, *J* = 7.8 Hz), 7.34 (t, 1H, *J* = 7.9 Hz), 3.84 (t, 2H, *J* = 7.2 Hz), 2.68 (s, 3H), 2.60 (t, 2H, *J* = 8.2 Hz), 2.28−2.32 (m, 2H). LCMS (ESI): *m*/*z*= 376 $(M+H)^+$.

Synthesis of 1-Cyclopropyl-3-(4-((2-oxopyrrolidin-1-yl)amino)-9H-pyrimido[4,5-b]indol-8-yl)urea Formic Acid Salt (AVI-4051). To a solution of 1-((8-amino-9H-pyrimido[4,5-*b*]indol-4-yl)amino)-pyrrolidin-2-one (20 mg, 0.071 mmol) and triethylamine (0.040 mL, 0.28 mmol) in THF (1 mL), was added cyclopropyl isocyanate (24 mg, 0.28 mmol). After stirring at 65 °C for 48 h, the reaction mixture was purified by reverse phase chromatography (water/acetonitrile/0.1% formic acid) to obtain 12 mg (41%) of **AVI-4051** formate as a white solid. ^{1}H NMR (DMSO-d_6, 400 MHz) δ 11.81 (br s, 1H), 9.31 (s, 1H), 8.50 (br s, 1H), 8.41 (s, 1H), 7.99 (d, 1H, *J* = 7.8 Hz), 7.63

https://doi.org/10.1021/acs.jmedchem.5c02933
J. Med. Chem. XXXX, XXX, XXX−XXX

(d, 1H, J = 7.8 Hz), 7.21 (t, 1H, J = 7.9 Hz), 6.74 (br s, 1H), 3.70 (br t, 2H, J = 7.1 Hz), 3.12−3.17 (m, 2H), 2.54−2.65 (m, 1H), 2.39−2.43 (m, 2H), 0.98 (t, 2H, J = 7.1 Hz), 0.68−0.70 (m, 2H). LCMS (ESI): m/z= 366 $(M+H)^+$.

Synthesis of 1-Cyclopentyl-3-(4-((2-oxopyrrolidin-1-yl)amino)-9H-pyrimido[4,5-b]indol-8-yl)urea (AVI-4057). To a solution of 1-((8-amino-9H-pyrimido[4,5-*b*]indol-4-yl)amino)pyrrolidin-2-one (20 mg, 0.071 mmol) and triethylamine (0.040 mL, 0.28 mmol) in THF (1 mL), was added cyclopentyl isocyanate (0.016 mL, 0.14 mmol). After stirring at 65 °C for 18 h, the reaction mixture was purified by reverse phase chromatography (water/acetonitrile/0.1% formic acid) to obtain 6 mg (20%) of **AVI-4057** formate as a white solid. ^{1}H NMR (DMSO-d_6, 400 MHz) δ 11.74 (br s, 1H), 9.31 (s, 1H), 8.41 (s, 1H), 7.97 (d, 1H, J = 7.8 Hz), 7.58 (d, 1H, J = 7.8 Hz), 7.35 (s, 1H), 7.20 (t, 1H, J = 7.9 Hz), 6.47 (br d, 1H, J = 7.1 Hz), 4.03−4.05 (m, 1H), 3.70 (t, 2H, J = 7.1 Hz), 2.41 (t, 2H, J = 8.0 Hz), 2.13 (br dd, 2H, J = 7.8, 15.6 Hz), 1.89 (br dd, 2H, J = 5.5, 12.1 Hz), 1.67−1.69 (m, 2H), 1.46−1.58 (m, 4H). LCMS (ESI): m/z= 394 $(M+H)^+$.

Synthesis of (R)-3-Methyl-2-((6-phenyl-7H-pyrrolo[2,3-d]-pyrimidin-4-yl)amino)butan-1-ol (AVI-4211). A mixture of (*R*)-2-((6-bromo-7*H*-pyrrolo[2,3-*d*]pyrimidin-4-yl)amino)-3-methylbutan-1-ol (15.0 mg, 50.1 μmol), phenylboronic acid (12.2 mg, 100.0 μmol), Pd(dppf)Cl_2 (3.7 mg, 5.01 μmol) and Cs_2CO_3 (40.8 mg, 125 μmol) in 0.22 mL of dioxane/H_2O (10:1) was stirred at 110 °C for 17 h. The residue was purified by prep-HPLC (0%−70% water/ACN with 0.1% formic acid) to give **AVI-4211** formate as a white solid (9.7 mg, yield: 57%). 1H NMR (400 MHz, MeOD) δ 8.41 (brs, 1H), 8.11 (s, 1H), 7.79 (brd, 1H, J = 8.0 Hz), 7.45 (brdd, 2H, J = 8.0, 7.5 Hz), 7.33 (brt, 1H, J = 7.5 Hz), 7.03 (s, 1H), 4.16−4.12 (m, 1H), 3.85−3.75 (m, 2H), 2.15−2.08 (m, 1H), 1.08−1.04 (m, 6H). LCMS (ESI): m/z = 297 $(M+H)^+$.

Synthesis of (R)-2-((6-(2-Fluorophenyl)-7H-pyrrolo[2,3-d]-pyrimidin-4-yl)amino)-3-methylbutan-1-ol (AVI-4678). A mixture of (*R*)-2-((6-bromo-7*H*-pyrrolo[2,3-*d*]pyrimidin-4-yl)amino)-3-methylbutan-1-ol (15.0 mg, 50.1 μmol), (2-fluorophenyl)boronic acid (14.0 mg, 100.0 μmol), Pd(dppf)Cl_2 (3.7 mg, 5.01 μmol) and Cs_2CO_3 (40.8 mg, 125 μmol) in 0.22 mL of of dioxane/H_2O (10:1) was stirred at 110 °C for 2 h. The residue was purified by prep-HPLC (0−70% water/ACN with 0.1% formic acid) to give **AVI-4678** formate as a white solid (10.9 mg, yield: 60%). 1H NMR (400 MHz, MeOD) δ 8.39 (brs, 1H), 8.13 (s, 1H), 7.83−7.78 (m, 1H), 7.37−7.20 (m, 3H), 7.16 (s, 1H), 4.17−4.12 (m, 1H), 3.86−3.75 (m, 2H), 2.17−2.07 (m, 1H), 1.08−1.03 (m, 6H). LCMS (ESI): m/z = 315 $(M+H)^+$.

Synthesis of (R)-2-((6-(2-Chlorophenyl)-7H-pyrrolo[2,3-d]-pyrimidin-4-yl)amino)-3-methylbutan-1-ol (AVI-4335). A mixture of (*R*)-2-((6-bromo-7*H*-pyrrolo[2,3-*d*]pyrimidin-4-yl)amino)-3-methylbutan-1-ol (15.0 mg, 50.1 μmol), (2-chlorophenyl)boronic acid (15.7 mg, 100.0 μmol), Pd(dppf)Cl_2 (3.7 mg, 5.01 μmol) and Cs_2CO_3 (40.8 mg, 125 μmol) in 0.22 mL of of dioxane/H_2O (10:1) was stirred at 110 °C for 1 h. The residue was purified by prep-HPLC (0−50% water/ACN with 0.1% formic acid) to give **AVI-4335** formate as a white solid (8.3 mg, yield: 44%). 1H NMR (400 MHz, MeOD) δ 8.16 (brs, 1H), 7.66 (brd, 1H, J = 7.7 Hz), 7.55 (brd, 1H, J = 7.9 Hz), 7.45−7.35 (m, 2H), 7.13 (s, 1H), 4.15−4.11 (m, 1H), 3.86−3.75 (m, 2H), 2.15−2.07 (m, 1H), 1.08−1.04 (m, 6H). LCMS (ESI): m/z = 331 $(M+H)^+$.

Synthesis of (R)-3-Methyl-2-((6-(o-tolyl)-7H-pyrrolo[2,3-d]-pyrimidin-4-yl)amino)butan-1-ol (AVI-4370). A mixture of (*R*)-2-((6-iodo-7H-pyrrolo[2,3-*d*]pyrimidin-4-yl)amino)-3-methylbutan-1-ol (15.0 mg, 43.3 μmol), *o*-tolylboronic acid (11.8 mg, 86.7 μmol), Pd(dppf)Cl_2 (3.2 mg, 4.3 μmol) and Cs_2CO_3 (35.3 mg, 108 μmol) in 0.22 mL of of dioxane/H_2O (10:1) was stirred at 110 °C for 1 h. The residue was purified by prep-HPLC (0−50% water/ACN with 0.1% formic acid) to give **AVI-4370** formate as a white solid (5.4 mg, yield: 35%). 1H NMR (400 MHz, MeOD) δ 8.35 (brs, 1H), 8.13 (s, 1H), 7.51−7.49 (m, 1H), 7.34−7.27 (m, 3H), 7.16−7.14 (brs, 1H), 6.68 (brs, 1H), 4.13−4.11 (m, 1H), 3.86−3.75 (m, 2H), 2.50 (s, 3H), 2.14−2.09 (m, 1H), 1.08−1.04 (m, 6H). LCMS (ESI): m/z = 311 $(M+H)^+$

Synthesis of (*R*)-2-(4-((1-hydroxy-3-methylbutan-2-yl)amino)-7H-pyrrolo[2,3-*d*]pyrimidin-6-yl)benzonitrile (AVI-4213). A mixture of (*R*)-2-((6-bromo-7*H*-pyrrolo[2,3-*d*]pyrimidin-4-yl)amino)-3-methylbutan-1-ol (15.0 mg, 50.1 μmol), (2-cyanophenyl)boronic acid (14.7 mg, 100.0 μmol), Pd(dppf)Cl_2 (3.7 mg, 5.01 μmol) and Cs_2CO_3 (40.8 mg, 125 μmol) in 0.22 mL of of dioxane/H_2O (10:1) was stirred at 110 °C for 4 h. The residue was purified by prep-HPLC (0−50% water/ACN) to give **AVI-4213** as a white solid (1.2 mg, yield: 7%). 1H NMR (400 MHz, MeOD) δ 8.52 (brs, 1H), 8.16 (s, 1H), 7.88−7.75 (m, 3H), 7.52 (ddd, 1H, J = 7.6, 7.6, 1.4 Hz), 7.33 (s, 1H), 4.21−4.14 (m, 1H), 3.85−3.75 (m, 2H), 2.14−2.09 (m, 1H), 1.08−1.04 (m, 6H). LCMS (ESI): m/z = 322 $(M+H)^+$.

Synthesis of (R)-3-Methyl-2-((6-(pyridin-3-yl)-7H-pyrrolo[2,3-d]-pyrimidin-4-yl)amino)butan-1-ol (AVI-4271). A mixture of (*R*)-2-((6-bromo-7*H*-pyrrolo[2,3-*d*]pyrimidin-4-yl)amino)-3-methylbutan-1-ol (15.0 mg, 50.1 μmol), pyridin-3-ylboronic acid (18.5 mg, 150.0 μmol), Pd(dppf)Cl_2 (7.4 mg, 10.0 μmol) and Cs_2CO_3 (40.8 mg, 125 μmol) in 0.22 mL of of dioxane/H_2O (10:1) was stirred at 110 °C for 24 h. The residue was purified by prep-HPLC (0−30% water/ACN with 0.1% formic acid) to give **AVI-4271** formate as a white solid (3.7 mg, yield: 22%). 1H NMR (400 MHz, MeOD) δ 8.98 (s, 1H), 8.48 (d, 1H, J = 4.8 Hz), 8.20 (d, 1H, J = 8.1 Hz), 8.13 (s, 1H), 7.52 (dd, 1H, J = 8.1, 4.7 Hz), 7.16 (brs, 1H), 4.18 (ddd, 1H, J = 7.6, 5.8, 4.1 Hz), 3.85−3.76 (m, 2H), 2.16−2.07 (m, 1H), 1.08−1.04 (m, 6H). LCMS (ESI): m/z = 298 $(M+H)^+$.

Synthesis of (R)-3-Methyl-2-((6-(pyrimidin-5-yl)-7H-pyrrolo[2,3-d]pyrimidin-4-yl)amino)butan-1-ol (AVI-4272). A mixture of (*R*)-2-((6-bromo-7*H*-pyrrolo[2,3-*d*]pyrimidin-4-yl)amino)-3-methylbutan-1-ol (15.0 mg, 50.1 μmol), pyrimidin-5-ylboronic acid (24.8 mg, 200.0 μmol), Pd(dppf)Cl_2 (18.4 mg, 25.1 μmol) and Cs_2CO_3 (40.8 mg, 125 μmol) in 0.22 mL of of dioxane/H_2O (10:1)was stirred at 110 °C for 4 days. The residue was purified by prep-HPLC (0−30% water/ACN with 0.1% formic acid) to give **AVI-4272** formate as a white solid (1.0 mg, yield: 6%). 1H NMR (400 MHz, MeOD) δ 9.19 (s, 2H), 9.08 (s, 1H), 8.48 (brs, 2H), 8.16 (s, 1H), 7.26 (s, 1H), 4.22−4.18 (m, 1H), 3.85−3.75 (m, 2H), 2.14−2.07 (m, 1H), 1.08−1.04 (m, 6H). LCMS (ESI): m/z = 299 $(M+H)^+$.

Synthesis of (R)-3-Methyl-2-((6-(thiophen-2-yl)-7H-pyrrolo[2,3-d]pyrimidin-4-yl)amino)butan-1-ol (AVI-4094). A mixture of (*R*)-2-((6-bromo-7*H*-pyrrolo[2,3-*d*]pyrimidin-4-yl)amino)-3-methylbutan-1-ol (15 mg, 50.1 μmol), thiophen-2-ylboronic acid (12.8 mg, 100.0 μmol), Pd(dppf)Cl_2 (3.7 mg, 5.01 μmol) and Cs_2CO_3 (40.8 mg, 125 μmol) in 0.22 mL of dioxane/H_2O (10:1) was stirred at 110 °C for 10 min. The residue was purified by prep-HPLC (0%−50% water/ACN with 0.1% formic acid) to give **AVI-4094** formate as a white solid (13.2 mg, yield: 87%). 1H NMR (400 MHz, MeOD) δ 8.30 (brs, 1H), 8.11 (s, 1H), 7.43 (dd, 1H, J = 3.6, 1.4 Hz), 7.39 (dd, 1H, J = 5.1, 1.4 Hz), 7.12−7.09 (m, 1H), 6.89 (s, 1H), 4.14−4.04 (m, 1H), 3.85−3.74 (m, 2H), 2.14−2.06 (m, 1H), 1.07−1.03 (m, 6H). LCMS (ESI): m/z = 303 $(M+H)^+$.

Synthesis of (R)-3-Methyl-2-((6-(thiophen-3-yl)-7H-pyrrolo[2,3-d]pyrimidin-4-yl)amino)butan-1-ol (AVI-4334). A mixture of (*R*)-2-((6-bromo-7*H*-pyrrolo[2,3-*d*]pyrimidin-4-yl)amino)-3-methylbutan-1-ol (15 mg, 50.1 μmol), thiophen-3-ylboronic acid (12.8 mg, 100.0 μmol), Pd(dppf)Cl_2 (3.7 mg, 5.01 μmol) and Cs_2CO_3 (40.8 mg, 125 μmol) in 0.22 mL of dioxane/H_2O (10:1) was stirred at 110 °C for 2 h. The residue was purified by prep-HPLC (0−60% water/ACN with 0.1% formic acid) to give **AVI-4334** formate as a white solid (10.5 mg, yield: 60%). 1H NMR (400 MHz, MeOD) δ 8.10 (s, 1H), 7.72−7.70 (m, 1H), 7.52−7.50 (m, 2H), 6.87 (brs, 1H), 4.13 (ddd, 1H, J = 7.5, 5.7, 4.1 Hz), 3.84−3.75 (m, 2H), 2.14−2.09 (m, 1H), 1.08−1.03 (m, 6H). LCMS (ESI): m/z = 303 $(M+H)^+$.

Synthesis of (R)-4-(4-((1-Hydroxy-3-methylbutan-2-yl)amino)-7H-pyrrolo[2,3-d]pyrimidin-6-yl)thiophene-3-carbonitrile (AVI-4684). A mixture of (*R*)-2-((6-iodo-7H-pyrrolo[2,3-*d*]pyrimidin-4-yl)amino)-3-methylbutan-1-ol (15.0 mg, 43.3 μmol), 4-(4,4,5,5-tetramethyl-1,3,2-dioxaborolan-2-yl)thiophene-3-carbonitrile (16.3 mg, 69.3 μmol), Pd(dppf)Cl_2 (3.2 mg, 4.33 μmol) and Cs_2CO_3 (35.3 mg, 108 μmol) in 0.22 mL of dioxane/H_2O (10:1) was stirred at 110 °C for 1 h. The residue was purified by prep-HPLC (0−80%

https://doi.org/10.1021/acs.jmedchem.5c02933
J. Med. Chem. XXXX, XXX, XXX−XXX

water/ACN) to give **AVI-4684** as a white solid (4.5 mg, yield: 32%). 1H NMR (400 MHz, *d*-DMSO) δ 12.0 (brs, 1H), 8.71 (d, 1H, J = 3.1 Hz), 8.11 (s, 1H), 8.02 (d, 1H, J = 3.1 Hz), 7.43 (brd, 1H, J = 8.6 Hz), 7.28 (s, 1H), 4.65−4.62 (m, 1H), 4.25−4.18 (m, 1H), 3.60−3.57 (m, 2H), 2.07−1.99 (m, 1H), 0.96−0.92 (m, 6H). LCMS (ESI): m/z = 328 $(M+H)^+$.

Synthesis of (R)-3-(4-((1-Hydroxy-3-methylbutan-2-yl)amino)-7H-pyrrolo[2,3-d]pyrimidin-6-yl)thiophene-2-carbonitrile (AVI-4683). A mixture of (*R*)-2-((6-iodo-7H-pyrrolo[2,3-*d*]pyrimidin-4-yl)amino)-3-methylbutan-1-ol (15.0 mg, 43.3 μmol), 3-(4,4,5,5-tetramethyl-1,3,2-dioxaborolan-2-yl)thiophene-2-carbonitrile (16.3 mg, 69.3 μmol), Pd(dppf)Cl_2 (3.2 mg, 4.33 μmol) and Cs_2CO_3 (35.3 mg, 108 μmol) in 0.22 mL of dioxane/H_2O (10:1) was stirred at 110 °C for 1 h. The residue was purified by prep-HPLC (0−60% water/ACN) to give **AVI-4683** as a white solid (5.3 mg, yield: 37%). 1H NMR (400 MHz, *d*-DMSO) δ 12.2 (brs, 1H), 8.15−8.12 (m, 2H), 7.74 (d, 1H, J = 5.2 Hz), 7.57 (brd, 1H, J = 8.7 Hz), 7.50 (s, 1H), 4.65−4.64 (m, 1H), 4.25−4.17 (m, 1H), 3.61−3.58 (m, 2H), 2.06−2.01 (m, 1H), 0.96−0.93 (m, 6H). LCMS (ESI): m/z = 328 $(M+H)^+$.

Synthesis of (R)-2-((6-(Furan-2-yl)-7H-pyrrolo[2,3-d]pyrimidin-4-yl)amino)-3-methylbutan-1-ol (AVI-4267). A mixture of (*R*)-2-((6-bromo-7*H*-pyrrolo[2,3-*d*]pyrimidin-4-yl)amino)-3-methylbutan-1-ol (15.0 mg, 50.1 μmol), 2-(furan-2-yl)-4,4,5,5-tetramethyl-1,3,2-dioxaborolane (19.5 mg, 100.0 μmol), Pd(dppf)Cl_2 (3.7 mg, 5.0 μmol) and Cs_2CO_3 (40.8 mg, 125 μmol) in 0.22 mL of dioxane/H_2O (10:1) was stirred at 110 °C for 5 min. The residue was purified by prep-HPLC (0−50% water/ACN with 0.1% formic acid) to give **AVI-4267** formate as a white solid (6.7 mg, yield: 40%). 1H NMR (400 MHz, MeOD) δ 8.11 (brs, 1H), 7.59−7.57 (m, 1H), 6.90 (m, 1H), 6.75 (m, 1H), 6.57−6.54 (m, 1H), 4.15−4.11 (m, 1H), 3.84−3.74 (m, 1H), 2.15−2.06 (m, 1H), 1.07−1.02 (m, 6H). LCMS (ESI): m/z = 287 $(M+H)^+$.

Synthesis of (R)-2-((6-(1H-Pyrrol-2-yl)-7H-pyrrolo[2,3-d]pyrimidin-4-yl)amino)-3-methylbutan-1-ol (AVI-4097). A mixture of (*R*)-2-((6-bromo-7*H*-pyrrolo[2,3-*d*]pyrimidin-4-yl)amino)-3-methylbutan-1-ol (15.0 mg, 50.1 μmol), (1-(tert-butoxycarbonyl)-1*H*-pyrrol-2-yl)boronic acid (21.2 mg, 100.0 μmol), Pd(dppf)Cl_2 (3.67 mg, 5.0 μmol) and Cs_2CO_3 (40.8 mg, 125 μmol) in 0.22 mL of dioxane/H_2O (10:1) was stirred at 110 °C for 24 h. The residue was purified by NP-column (CH_2CL_2/MeOH 95:5 with NH_3) to give *tert*-butyl (*R*)-2-(4-((1-hydroxy-3-methylbutan-2-yl)amino)-7*H*-pyrrolo[2,3-*d*]pyrimidin-6-yl)-1*H*-pyrrole-1-carboxylate as a brown solid (11.9 mg, yield: 62%). LCMS (ESI): m/z = 386 $(M+H)^+$.

Add solution of *tert*-butyl (*R*)-2-(4-((1-hydroxy-3-methylbutan-2-yl)amino)-7*H*-pyrrolo[2,3-*d*]pyrimidin-6-yl)-1*H*-pyrrole-1-carboxylate (11.9 mg, 30.9 μmol) in 0.20 mL of methanol dropwise at 0 °C to a solution of acetyl chloride (44.0 μL, 618 mmol) and the reaction mixture stirred 2 days at room temperature. The reaction mixture was concentrated and the residue washed with 7 M NH_3 in MeOH and evaporated three times repeatedly. The residue was purified by prep-HPLC (0−50% water/ACN with 0.1% formic acid) to give **AVI-4097** formate as a white solid (5.8 mg, yield: 66%). 1H NMR (400 MHz, MeOD) δ 8.31 (brs, 1H), 8.07 (brs, 1H), 6.87−6.86 (m, 1H), 6.68−6.66 (m, 1H), 6.57−6.55 (m, 1H), 6.21−6.19 (m, 1H), 4.10−4.04 (m, 1H), 3.85−3.75 (m, 2H), 2.17−2.04 (m, 1H), 1.08−1.04 (m, 6H). LCMS (ESI): m/z = 286 $(M+H)^+$.

Synthesis of (R)-2-((6-(1H-Indol-6-yl)-7H-pyrrolo[2,3-d]pyrimidin-4-yl)amino)-3-methylbutan-1-ol (AVI-4212). A mixture of (*R*)-2-((6-bromo-7*H*-pyrrolo[2,3-*d*]pyrimidin-4-yl)amino)-3-methylbutan-1-ol (15.0 mg, 50.1 μmol), (1*H*-indol-6-yl)boronic acid (16.1 mg, 200.0 μmol), Pd(dppf)Cl_2 (3.7 mg, 5.01 μmol) and Cs_2CO_3 (40.8 mg, 125 μmol) in 0.22 mL of dioxane/H_2O (10:1)was stirred at 110 °C for 17 h. The residue was purified by prep-HPLC (0−50% water/ACN with 0.1% formic acid) to give **AVI-4212** formate as a white solid (8.1 mg, yield: 42%). 1H NMR (400 MHz, MeOD) δ 8.43 (brs, 1H), 8.10 (s, 1H), 7.81 (s, 1H), 7.62 (d, 1H, J = 8.3 Hz), 7.48 (d, 1H, J = 8.3 Hz), 7.30 (d, 1H, J = 3.1 Hz), 6.97 (s, 1H), 6.48 (d, 1H, J = 3.1 Hz), 4.14−4.10 (m, 1H), 3.87−3.76 (m, 2H), 2.17−2.08 (m, 1H), 1.09−1.05 (m, 6H). LCMS (ESI): m/z = 336 $(M+H)^+$.

Synthesis of (R)-2-((6-(1H-Pyrazol-5-yl)-7H-pyrrolo[2,3-d]pyrimidin-4-yl)amino)-3-methylbutan-1-ol (AVI-4099). A mixture of (*R*)-2-((6-bromo-7*H*-pyrrolo[2,3-*d*]pyrimidin-4-yl)amino)-3-methylbutan-1-ol (10.0 mg, 33.4 μmol), 5-(4,4,5,5-tetramethyl-1,3,2-dioxaborolan-2-yl)-1*H*-pyrazole (13.0 mg, 66.9 μmol), Pd(dppf)Cl_2 (4.9 mg, 6.7 μmol) and CsOH (12.5 mg, 83.6 μmol) in 0.25 mL of ^{n}BuOH/H_2O (4:1) was stirred at 130 °C for 20 min with microwave. The residue was purified by prep-HPLC (0−30% water/ACN with 0.1% formic acid) to give **AVI-4099** formate as a white solid (3.7 mg, yield: 39%). 1H NMR (400 MHz, MeOD) δ 8.42 (brs, 1H), 8.12 (brs, 1H), 7.73 (d, 1H, J = 2.3 Hz), 6.97 (s, 1H), 6.72 (d, 1H, J = 2.3 Hz), 4.16−4.11 (m, 1H), 3.84−3.75 (m, 2H), 2.16−2.06 (m, 1H), 1.09−1.02 (m, 6H). LCMS (ESI): m/z = 287 $(M+H)^+$.

Synthesis of (R)-2-((6-(1H-Pyrazol-4-yl)-7H-pyrrolo[2,3-d]pyrimidin-4-yl)amino)-3-methylbutan-1-ol (AVI-4268). A mixture of (*R*)-2-((6-bromo-7*H*-pyrrolo[2,3-*d*]pyrimidin-4-yl)amino)-3-methylbutan-1-ol (15.0 mg, 50.1 μmol), (1*H*-pyrazol-4-yl)boronic acid (22.4 mg, 200.0 μmol), Pd(dppf)Cl_2 (7.3 mg, 10.0 μmol) and Cs_2CO_3 (40.8 mg, 125 μmol) in 0.22 mL of dioxane/H_2O (10:1)was stirred at 110 °C for 4 days. The residue was purified by prep-HPLC (0−40% water/ACN with 0.1% formic acid) to give **AVI-4268** formate as a white solid (2.7 mg, yield: 16%). 1H NMR (400 MHz, MeOD) δ 8.48 (brs, 1H), 8.15−8.14 (m, 2H), 7.77 (m, 1H), 6.71 (s, 1H), 6.57 (m, 1H), 4.18−4.14 (m, 1H), 3.84−3.74 (m, 2H), 2.16−2.01 (m, 1H), 1.07−1.03 (m, 6H). LCMS (ESI): m/z = 287 $(M+H)^+$.

Synthesis of (R)-3-Methyl-2-((6-(1-methyl-1H-pyrazol-4-yl)-7H-pyrrolo[2,3-d]pyrimidin-4-yl)amino)butan-1-ol (AVI-4214). A mixture of (*R*)-2-((6-bromo-7*H*-pyrrolo[2,3-*d*]pyrimidin-4-yl)amino)-3-methylbutan-1-ol (15.0 mg, 50.1 μmol), (1-methyl-1*H*-pyrazol-4-yl)boronic acid (12.6 mg, 100.0 μmol), Pd(dppf)Cl_2 (3.7 mg, 5.01 μmol) and Cs_2CO_3 (40.8 mg, 125 μmol) in 0.22 mL of dioxane/H_2O (10:1) was stirred at 110 °C for 4 h. The residue was purified by prep-HPLC (0−50% water/ACN with 0.1% formic acid) to give **AVI-4214** formate as a white solid (11.1 mg, yield: 64%). 1H NMR (400 MHz, MeOD) δ 8.29 (brs, 1H), 8.08 (s, 1H), 7.97 (s, 1H), 7.86 (s, 1H), 6.75 (brs, 1H), 4.10−4.05 (m, 1H), 3.96 (s, 3H), 3.86−3.74 (m, 2H), 2.14−2.06 (m, 1H), 1.09−1.03 (m, 6H). LCMS (ESI): m/z = 301 $(M+H)^+$.

Synthesis of (R)-2-((6-(1,5-Dimethyl-1H-pyrazol-4-yl)-7H-pyrrolo[2,3-d]pyrimidin-4-yl)amino)-3-methylbutan-1-ol (AVI-4266). A mixture of (*R*)-2-((6-bromo-7*H*-pyrrolo[2,3-*d*]pyrimidin-4-yl)amino)-3-methylbutan-1-ol (15.0 mg, 50.1 μmol), 1,5-dimethyl-4-(4,4,5,5-tetramethyl-1,3,2-dioxaborolan-2-yl)-1*H*-pyrazole (44.6 mg, 200.0 μmol), Pd(dppf)Cl_2 (7.3 mg, 10.0 μmol) and Cs_2CO_3 (40.8 mg, 125 μmol) in 0.22 mL of dioxane/H_2O (10:1) was stirred at 110 °C for 2 days. The residue was purified by prep-HPLC (0−50% water/ACN with 0.1% formic acid) to give **AVI-4266** formate as a white solid (4.1 mg, yield: 23%). 1H NMR (400 MHz, MeOD) δ 8.52 (brs, 1H), 8.08 (s, 1H), 7.74 (s, 1H), 6.67 (s, 1H), 4.15−4.10 (m, 1H), 3.88−3.87 (m, 3H), 3.84−3.74 (m, 2H), 2.53−2.52 (m, 3H), 2.14−2.07 (m, 1H), 1.07−1.03 (m, 6H). LCMS (ESI): m/z = 315 $(M+H)^+$.

Synthesis of (R)-4-(4-((1-Hydroxy-3-methylbutan-2-yl)amino)-7H-pyrrolo[2,3-d]pyrimidin-6-yl)-1-methyl-1H-pyrazole-5-carbonitrile (AVI-4054). To a solution of 4-(4-chloro-7H-pyrrolo[2,3-*d*]pyrimidin-6-yl)-1-methyl-1H-pyrazole-5-carbonitrile (70 mg, 0.27 mmol) in dry DMSO (2 mL) was added (*R*)-2-amino-3-methylbutan-1-ol (42.23 mg, 0.41 mmol) and triethylamine (72.4 mg, 0.81 mmol). After stirring at 100 °C for 16 h, the mixture was diluted with ethyl acetate (40.0 mL) and washed with water (5.0 mL) and brine (5.0 mL). The organic layer was dried over Na_2SO_4 and concentrated under reduced pressure. The residue was purified by prep-HPLC (10−100% 0.1% NH_4HCO_3 in water/ACN) to give **AVI-4054** as a white solid (25.4 mg, yield: 28.8%). 1H NMR (500 MHz, MeOD) δ 8.09 (s, 1H), 7.98 (s, 1H), 7.13 (s, 1H), 4.14 (s, 1H), 4.09 (s, 3H), 3.77 (dd, J = 13.4, 5.0 Hz, 2H), 2.08 (dt, J = 13.8, 6.9 Hz, 1H), 1.02 (dd, J = 13.2, 6.8 Hz, 6H). LCMS (ESI): m/z 326.1 $(M+H)^+$.

(R)-4-(4-((1-Hydroxy-3-methylbutan-2-yl)amino)-7H-pyrrolo[2,3-d]pyrimidin-6-yl)-1-methyl-1H-pyrazole-3-carbonitrile (AVI-5707).

https://doi.org/10.1021/acs.jmedchem.5c02933
J. Med. Chem. XXXX, XXX, XXX−XXX

A mixture of (*R*)-2-((6-iodo-7H-pyrrolo[2,3-*d*]pyrimidin-4-yl)-amino)-3-methylbutan-1-ol (15 mg, 43.3 umol), 1-methyl-4-(4,4,5,5-tetramethyl-1,3,2-dioxaborolan-2-yl)-1H-pyrazole-3-carbonitrile (16.2 mg, 69.3 umol), Pd(dppf)Cl_2 (3.2 mg, 4.33 umol) and $CsCO_3$ (35.3 mg, 108 mmol) in 0.22 mL of dioxane/H_2O (10:1) was stirred at 110 °C for 1 h. Subsequently, the mixture was extracted thrice with EtOAc, the combined organic phase was washed with brine, dried over Na2SO4 and concentrated in vacuo. The residue was purified by silica gel chromatography (20−40% EtOAc in hexane and prep-HPLC, 2.1 mg (13%) of **AVI-5707** formate as a white solid. 1H NMR (DMSO-d6, 400 MHz) δ 11.96−12.03 (m, 1H), 8.44 (br s, 1H), 8.28−8.30 (m, 1H), 8.08 (s, 1H), 7.40 (br d, 1H, J = 8.0 Hz), 7.14 (s, 1H), 4.19 (br s, 1H), 4.00 (s, 3H), 3.57−3.61 (m, 2H), 2.02 (qd, 1H, J = 6.7, 13.6 Hz), 1.24 (s, 1H), 0.94 (t, 6H, J = 6.5 Hz). LCMS (ESI): m/z = 326 $(M+H)^+$.

Synthesis of (R)-2-((6-(Isothiazol-5-yl)-7H-pyrrolo[2,3-d]-pyrimidin-4-yl)amino)-3-methylbutan-1-ol (AVI-4100). A mixture of (*R*)-2-((6-bromo-7*H*-pyrrolo[2,3-*d*]pyrimidin-4-yl)amino)-3-methylbutan-1-ol (10.0 mg, 33.4 μmol), 5-(4,4,5,5-tetramethyl-1,3,2-dioxaborolan-2-yl)isothiazole (14.1 mg, 66.9 μmol), Pd$(PPh_3)_4$ (7.7 mg, 6.7 μmol) and Na_2CO_3 (7.09 mg, 66.9 μmol) in 0.22 mL of dioxane/H_2O (10:1) was stirred at 110 °C for 24 h. The residue was purified by prep-HPLC (0−40% water/ACN with 0.1% formic acid) to give **AVI-4100** formate as a white solid (1.2 mg, yield: 10%). 1H NMR (400 MHz, MeOD) δ 8.55 (brs, 1H), 8.49 (d, 1H, J = 1.9 Hz), 8.15 (s, 1H), 7.63 (d, 1H, J = 1.9 Hz), 7.14 (s, 1H), 4.19−4.18 (m, 1H), 3.83−3.74 (m, 2H), 2.13−2.08 (m, 1H), 1.07−1.03 (m, 6H). LCMS (ESI): m/z = 304 $(M+H)^+$.

Synthesis of 4-(4-((2,2-Dimethyl-5-oxopyrrolidin-1-yl)amino)-7H-pyrrolo[2,3-d]pyrimidin-6-yl)-1-methyl-1H-pyrazole-5-carbonitrile (AVI-4052). A solution of 4-(4-chloro-7H-pyrrolo[2,3-*d*]-pyrimidin-6-yl)-1-methyl-1H-pyrazole-5-carbonitrile (70 mg, 0.27 mmol) and 1-amino-5,5-dimethylpyrrolidin-2-one (63.76 mg, 0.41 mmol) in iPrOH (2 mL) and HCl (1 drop) was stirred at 100 °C for 16 h. The reaction mixture was suspended in water (30 mL × 3) and extracted with ethyl acetate (3 × 60 mL). The organic layer was dried over Na_2SO_4 and concentrated under reduced pressure. The residue was purified by prep-HPLC (10−100% 0.1% NH_4HCO_3 in water/ACN) to **AVI-4052** as a white solid (25.1 mg, yield: 26.4%). 1H NMR (500 MHz, MeOD) δ 8.32 (s, 1H), 8.04 (s, 1H), 7.34 (s, 1H), 4.12 (s, 3H), 2.60 (d, J = 7.7 Hz, 2H), 2.22 (s, 2H), 1.37 (s, 6H). LCMS (ESI): m/z 351.1 $(M+H)^+$.

Synthesis of 4-(4-((2,2-Dimethyl-6-oxopiperidin-1-yl)amino)-7H-pyrrolo[2,3-d]pyrimidin-6-yl)-1-methyl-1H-pyrazole-5-carbonitrile (AVI-6320). To a solution of 4-(4-chloro-7H-pyrrolo[2,3-*d*]pyrimidin-6-yl)-1-methyl-1H-pyrazole-5-carbonitrile (120 mg, 0.46 mmol) in IPA (5 mL) was added 1-amino-6,6-dimethylpiperidin-2-one (99 mg, 0.70 mmol) and conc. HCl (0.04 mL). After stirring at 100 °C for 24 h, aqueous, saturated sodium bicarbonate (5 mL) was added to the reaction mixture and extracted with $_{DCM}$ (20 mL × 3), organic layers were separated and concentrated in vacuo, and purified by preprarative HPLC (10−40% 0.1% NH_4HCO_3 in water/ACN) to obtain **AVI-6320** as a white solid (24 mg, Yield: 14.45%). ^{1}H NMR (400 MHz, DMSO) δ 12.11 (s, 1H), 9.15 (s, 1H), 8.15 (d, J = 12.7 Hz, 2H), 6.92 (s, 1H), 4.04 (s, 3H), 2.68−2.52 (m, 1H), 2.39−2.25 (m, 1H), 2.05 (s, 1H), 1.84 (d, J = 5.5 Hz, 3H), 1.30 (d, J = 26.5 Hz, 6H). LCMS (ESI): m/z= 365.3 $(M+H)^+$.

Synthesis of 4-(4-((4,4-Dimethyl-2-oxooxazolidin-3-yl)amino)-7H-pyrrolo[2,3-d]pyrimidin-6-yl)-1-methyl-1H-pyrazole-5-carbonitrile (AVI-6318). To a solution of 4-(4-chloro-7-((2-(trimethylsilyl)-ethoxy)methyl)-7H-pyrrolo[2,3-*d*]pyrimidin-6-yl)-1-methyl-1H-pyrazole-5-carbonitrile (200 mg, 0.52 mmol) in IPA (5 mL) were added 3-amino-4,4-dimethyloxazolidin-2-one (98 mg, 0.75 mmol) and conc. HCl (0.04 mL). After stirring at 100 °C for 24 h, aqueous saturated sodium bicarbonate (5 mL) was added to the reaction mixture and extracted with DCM (20 mL × 3), organic layers were separated and concentrated in vacuo and purified by silica gel chromatography (dichloromethane/methanol, 10:1) to obtain 4-(4-((4,4-dimethyl-2-oxooxazolidin-3-yl)amino)-7-((2-(trimethylsilyl)ethoxy)methyl)-7H-pyrrolo[2,3-*d*]pyrimidin-6-yl)-1-methyl-1H-pyrazole-5-carbonitrile (55 mg, Yield: 21.9%) as a white solid. LCMS (ESI): m/z= 483.2 $(M+H)^+$.

To a solution of the intermediate above (55 mg, 0.11 mmol) in DCM (2.0 mL) was added TFA (0.5 mL). After stirring at 20 °C for 4 h, the reaction mixture was concentrated to dryness, the resulting residue was suspended in aqueous saturated NaHCO3 and extracted with DCM (10 mL × 3). The organic layers were washed with brine, concentrated under reduced pressure and purified by preparative HPLC (10−50% 0.1% NH_4HCO_3 in water/ACN) to obtain **AVI-6318** as a white solid (20 mg, Yield: 29.8%). ^{1}H NMR (500 MHz, DMSO) δ 12.44 (s, 1H), 9.76 (s, 1H), 8.25 (s, 1H), 8.17 (s, 1H), 7.08 (s, 1H), 4.41−4.15 (m, 2H), 4.07 (s, 3H), 1.31 (d, J = 11.9 Hz, 6H). LCMS (ESI): m/z= 353.1 $(M+H)^+$.

Synthesis of 1-Methyl-4-(4-((2-oxo-3,8-dioxa-1-azaspiro[4.5]-decan-1-yl)amino)-7H-pyrrolo[2,3-d]pyrimidin-6-yl)-1H-pyrazole-5-carbonitrile (AVI-6319). To a solution of 4-(4-chloro-7-((2-(trimethylsilyl)ethoxy)methyl)-7H-pyrrolo[2,3-*d*]pyrimidin-6-yl)-1-methyl-1H-pyrazole-5-carbonitrile (200 mg, 0.52 mmol) in IPA (5 mL) were added 1-amino-3,8-dioxa-1-azaspiro[4.5]decan-2-one (129 mg, 0.75 mmol) and conc. HCl (0.04 mL). After stirring at 100 °C for 24 h, aqueous saturated sodium bicarbonate (5 mL) was added to the reaction mixture and extracted with DCM (20 mL × 3), organic layers were separated and concentrated in vacuo and purified by silica gel chromatography (dichloromethane/methanol, 10:1) to obtain 1-methyl-4-(4-((2-oxo-3,8-dioxa-1-azaspiro[4.5]decan-1-yl)amino)-7-((2-(trimethylsilyl)ethoxy)methyl)-7H-pyrrolo[2,3-*d*]pyrimidin-6-yl)-1H-pyrazole-5-carbonitrile (60 mg, Yield: 22%) as a white solid. LCMS (ESI): m/z= 525.3 $(M+H)^+$.

To a solution of the intermediate above (60 mg, 0.11 mmol) in DCM (2.0 mL) was added TFA (0.5 mL). After stirring at 20 °C for 4 h, the reaction mixture was concentrated to dryness, the resulting residue was suspended in aqueous saturated NaHCO3 and extracted with DCM (10 mL × 3). The organic layers were washed with brine, concentrated under reduced pressure and purified by preparative HPLC (10−50% 0.1% NH_4HCO_3 in water/ACN) to obtain **AVI-6319** as a white solid (27 mg, yield: 62.3%). ^{1}H NMR (500 MHz, DMSO) δ 12.47 (s, 1H), 9.88 (s, 1H), 8.25 (s, 1H), 8.18 (s, 1H), 7.13 (s, 1H), 4.50 (d, J = 76.4 Hz, 2H), 4.07 (s, 3H), 3.91 (dd, J = 11.8, 4.2 Hz, 1H), 3.78 (d, J = 9.5 Hz, 1H), 3.46 (s, 1H), 3.26 (d, J = 12.2 Hz, 1H), 1.96 (td, J = 12.9, 4.7 Hz, 1H), 1.85 (s, 1H), 1.76−1.56 (m, 2H). LCMS (ESI): m/z = 395.1 $(M+H)^+$.

Synthesis of 1-Methyl-4-(4-((2-oxo-3-oxa-1,8-diazaspiro[4.5]-decan-1-yl)amino)-7H-pyrrolo[2,3-d]pyrimidin-6-yl)-1H-pyrazole-5-carbonitrile (AVI-6345). To a solution of 4-(4-chloro-7H-pyrrolo-[2,3-*d*]pyrimidin-6-yl)-1-methyl-1H-pyrazole-5-carbonitrile (500 mg, 1.93 mmol) in IPA (15 mL) were added benzyl 1-amino-2-oxo-3-oxa-1,8-diazaspiro[4.5]decane-8-carboxylate (707 mg, 2.32 mmol) and conc. HCl (0.06 mL). After stirring at 100 °C for 24 h, aqueous saturated sodium bicarbonate (5 mL) was added to the reaction mixture and extracted with DCM (20 mL × 3), organic layers were separated and concentrated in vacuo and purified by silica gel chromatography (dichloromethane/methanol, 10:1) to obtain benzyl 1-((6-(5-cyano-1-methyl-1H-pyrazol-4-yl)-7H-pyrrolo[2,3-*d*]-pyrimidin-4-yl)amino)-2-oxo-3-oxa-1,8-diazaspiro[4.5]decane-8-carboxylate (30 mg, Yield: 2.9%) as a white solid. LCMS (ESI): m/z = 528.1 $(M+H)^+$.

To a solution of the intermediate above (30 mg, 0.057 mmol) in acetonitrile (2.0 mL) was added TMSI (23 mg, 0.114 mmol). After stirring at 20 °C for 4 h, the reaction mixture was concentrated to dryness, the resulting residue was suspended in aqueous saturated NaHCO3 and extracted with DCM (10 mL × 3). The organic layers were washed with brine, concentrated under reduced pressure and purified by prep-TLC (DCM/MeOH = 10/1) to obtain **AVI-6345** as a white solid (6 mg, Yield: 26.8%). 1H NMR (500 MHz, DMSO) δ 12.44 (s, 1H), 9.85 (s, 1H), 8.24 (s, 1H), 8.17 (s, 1H), 7.13 (s, 1H), 4.39 (d, J = 69.5 Hz, 2H), 4.06 (s, 3H), 2.95 (d, J = 12.4 Hz, 1H), 2.82 (d, J = 12.5 Hz, 1H), 2.64−2.62 (m, 1H), 2.54−2.32 (m, 2H), 1.92−1.70 (m, 2H), 1.60−1.52 (m, 2H). LCMS (ESI): m/z= 394.1 $(M+H)^+$.

https://doi.org/10.1021/acs.jmedchem.5c02933
J. Med. Chem. XXXX, XXX, XXX−XXX

Synthesis of 1-Methyl-4-(4-((8-(methylsulfonyl)-2-oxo-3-oxa-1,8-diazaspiro[4.5]decan-1-yl)amino)-7H-pyrrolo[2,3-d]pyrimidin-6-yl)-1H-pyrazole-5-carbonitrile (AVI-6344). To a solution of 4-(4-chloro-7H-pyrrolo[2,3-*d*]pyrimidin-6-yl)-1-methyl-1H-pyrazole-5-carbonitrile (100 mg, 0.39 mmol) in IPA (5 mL) were added 1-amino-8-(methylsulfonyl)-3-oxa-1,8-diazaspiro[4.5]decan-2-one (149 mg, 0.60 mmol) and conc. HCl (0.04 mL). After stirring at 100 °C for 24 h, aqueous saturated sodium bicarbonate (5 mL) was added to the reaction mixture and extracted with DCM (20 mL × 3), organic layers were separated and concentrated in vacuo and purified by prep-HPLC (10−50% 0.1% NH4HCO3 in water/ACN) to obtain **AVI-6344** as a white solid (22 mg, yield: 12.0%). 1H NMR (500 MHz, DMSO) δ 12.47 (s, 1H), 9.88 (s, 1H), 8.25 (s, 1H), 8.18 (s, 1H), 7.02 (d, J = 100.1 Hz, 1H), 4.78−4.20 (m, 2H), 4.07 (s, 3H), 3.63 (d, J = 12.0 Hz, 1H), 3.50 (d, J = 12.2 Hz, 1H), 2.93 (s, 1H), 2.86 (s, 3H), 2.76 (dd, J = 22.8, 12.0 Hz, 1H), 2.16−1.89 (m, 3H), 1.76 (d, J = 65.1 Hz, 2H). LCMS (ESI): m/z = 472.0 $(M+H)^+$.

Synthesis of 4-(4-(((((trans)-2-Hydroxycyclopentyl)methyl)-amino)-7H-pyrrolo[2,3-d]pyrimidin-6-yl)-1-methyl-1H-pyrazole-5-carbonitrile (AVI-6315). To a solution of 4-(4-chloro-7-((2-(trimethylsilyl)ethoxy)methyl)-7H-pyrrolo[2,3-*d*]pyrimidin-6-yl)-1-methyl-1H-pyrazole-5-carbonitrile (500 mg, 1.29 mmol) in dry DMSO (10 mL) were added 2-(aminomethyl)cyclopentan-1-ol (223 mg, 1.93 mmol) and TEA (651 mg, 6.44 mmol) After stirring at 110 °C for 3 h, the reaction mixture was diluted with ethyl acetate (100.0 mL) and washed with water (10.0 mL), brine (10.0 mL). The organic layers were dried over Na_2SO_4 and concentrated under reduced pressure. The residue was purified by prep-HPLC (10−60% 10 mmol NH_4HCO_3 in water/ACN) to obtain trans and cis diastereomers.

4-(4-((((*trans*)-2-Hydroxycyclopentyl)methyl)amino)-7-((2-(trimethylsilyl)ethoxy)methyl)-7H-pyrrolo[2,3-*d*]pyrimidin-6-yl)-1-methyl-1H-pyrazole-5-carbonitrile as a white solid (200 mg, yield: 33.2%). ^{1}H NMR (500 MHz, DMSO) δ 8.32 (s, 1H), 8.20 (s, 1H), 7.97 (s, 1H), 7.18 (s, 1H), 5.69 (d, J = 11.3 Hz, 2H), 4.66 (d, J = 4.3 Hz, 1H), 4.21 (s, 3H), 3.99−3.91 (m, 1H), 3.66 (dd, J = 14.3, 6.3 Hz, 2H), 3.64−3.58 (m, 1H), 3.52−3.46 (m, 1H), 2.23−2.15 (m, 1H), 1.99−1.86 (m, 2H), 1.81−1.55 (m, 3H), 1.40 (td, J = 15.1, 7.2 Hz, 1H), 0.98−0.91 (m, 2H), −0.00 (d, J = 3.1 Hz, 9H). LCMS (ESI): m/z = 468.2 $(M+H)^+$.

4-(4-((((*cis*)-2-Hydroxycyclopentyl)methyl)amino)-7-((2-(trimethylsilyl)ethoxy)methyl)-7H-pyrrolo[2,3-*d*]pyrimidin-6-yl)-1-methyl-1H-pyrazole-5-carbonitrile as a white solid (120 mg, yield: 20%). ^{1}H NMR (500 MHz, DMSO) δ 8.32 (s, 1H), 8.20 (s, 1H), 8.06 (s, 1H), 7.17 (s, 1H), 5.72−5.65 (m, 2H), 5.03 (s, 1H), 4.22 (s, 3H), 4.09 (d, J = 20.0 Hz, 1H), 3.78−3.70 (m, 1H), 3.66 (t, J = 7.9 Hz, 2H), 3.60−3.51 (m, 1H), 2.18−2.07 (m, 1H), 1.90−1.74 (m, 3H), 1.74−1.49 (m, 3H), 0.98−0.91 (m, 2H), −0.01 (d, J = 5.7 Hz, 9H). LCMS (ESI): m/z = 468.1 $(M+H)^+$.

To a solution of the *trans* diastereomer above (80 mg, 0.17 mmol) in DCM (3 mL) was added TFA (1 mL). After stirring at 20 °C for 4 h, the reaction mixture was then concentrated to dryness. To the resulting residue was added saturated aqueous $NaHCO_3$ (5 mL) and extracted with DCM (30 mL × 2). The organic layers were washed with brine and concentrated under reduced pressure. The crude was purified by prep-HPLC (10−60% 10 mmol NH_4HCO_3 in water/ACN) to obtain **AVI-6315** as a white solid (30 mg, yield: 51.9%). ^{1}H NMR (500 MHz, DMSO) δ 12.09 (s, 1H), 8.13 (d, J = 2.0 Hz, 2H), 7.75 (s, 1H), 7.06 (s, 1H), 4.54 (d, J = 4.3 Hz, 1H), 4.05 (s, 3H), 3.87−3.76 (m, 1H), 3.50−3.43 (m, 1H), 3.37 (d, J = 6.5 Hz, 1H), 2.15−1.99 (m, 1H), 1.89−1.71 (m, 2H), 1.70−1.43 (m, 3H), 1.28 (dt, J = 15.2, 7.2 Hz, 1H). LCMS (ESI): m/z = 338.1 $(M+H)^+$.

Synthesis of 4-(4-((((cis)-2-Hydroxycyclopentyl)methyl)amino)-7H-pyrrolo[2,3-d]pyrimidin-6-yl)-1-methyl-1H-pyrazole-5-carbonitrile (AVI-6316). To a solution of the *cis* diastereomer (80 mg, 0.17 mmol) in DCM (3.0 mL) was added TFA (1.0 mL). After stirring at 20 °C for 4 h, the reaction mixture was then concentrated to dryness. To the resulting residue was added saturated aqueous NaHCO3 (5 mL) and extracted with DCM (30 mL × 2). The organic layers were washed with brine and concentrated under reduced pressure. The crude was purified by prep-HPLC (10−60% 10 mmol NH_4HCO_3 in water/ACN) to obtain **AVI-6316** as a white solid (28 mg, yield: 48.5%). ^{1}H NMR (500 MHz, DMSO) δ 12.14 (s, 1H), 8.12 (d, J = 7.4 Hz, 2H), 7.84 (s, 1H), 7.05 (s, 1H), 5.00 (s, 1H), 4.05 (s, 3H), 3.97 (s, 1H), 3.68−3.56 (m, 1H), 3.47−3.36 (m, 1H), 2.05−1.92 (m, 1H), 1.82−1.62 (m, 3H), 1.62−1.33 (m, 3H). LCMS (ESI): m/z= 338.1 $(M+H)^+$.

Synthesis of 1-Methyl-4-(4-(((2-oxocyclopentyl)methyl)amino)-7H-pyrrolo[2,3-d]pyrimidin-6-yl)-1H-pyrazole-5-carbonitrile (AVI-6317). To a cooled (−78 °C) solution of oxalyl chloride (82 mg, 0.64 mmol) in DCM (3 mL) was added DMSO (82 mg, 1.07 mmol) in DCM (1 mL) dropwise while stirring at under nitrogen gas. After 30 min, 4-(4-((((*trans*)-2-hydroxycyclopentyl)methyl)amino)-7-((2-(trimethylsilyl)ethoxy)methyl)-7H-pyrrolo[2,3-*d*]pyrimidin-6-yl)-1-methyl-1H-pyrazole-5-carbonitrile (200 mg, 0.43 mmol) in DCM (1 mL) was added dropwise and the mixture was stirred for an additional 90 min at −78 °C. Triethylamine (433 mg, 4.3 mmol) was then added dropwise and the reaction mixture was allowed to warm to room temperature. To this mixture was added water (10 mL) and extracted with DCM (10 mL × 3). The organic layers were washed with water, dried over Na_2SO_4, filtered, and concentrated under reduced pressure. The residue was purified by prep-HPLC (10 mmol NH_4HCO_3 in water, 10−60% MeCN) to obtain 1-methyl-4-(4-(((2-oxocyclopentyl)methyl)amino)-7-((2-(trimethylsilyl)ethoxy)methyl)-7H-pyrrolo[2,3-*d*]pyrimidin-6-yl)-1H-pyrazole-5-carbonitrile (90 mg, Yield: 45.2%) as a white solid. LCMS (ESI): m/z= 466 $(M+H)^+$.

To a solution of the intermediate above (80 mg, 0.19 mmol) in DCM (3 mL) was added TFA (1 mL). After stirring at 20 °C for 4h, the reaction mixture was concentrated to dryness. To the resulting residue was added saturated aqueous $NaHCO_3$ (5 mL) and extracted with DCM (30 mL × 2). The organic layers were washed with brine and concentrated under reduced pressure. The crude was purified by prep-HPLC (10−100% 10 mmol NH_4HCO_3 in water/ACN) to obtain **AVI-6317** as a white solid (28 mg, yield: 40.7%). ^{1}H NMR (500 MHz, DMSO) δ 12.07 (s, 1H), 8.14 (d, J = 3.9 Hz, 2H), 7.89 − 7.74 (m, 1H), 7.06 (s, 1H), 4.05 (s, 3H), 3.85 (dt, J = 13.2, 5.4 Hz, 1H), 3.37 (dd, J = 8.1, 5.7 Hz, 1H), 2.67−2.52 (m, 1H), 2.28−2.05 (m, 3H), 1.98−1.85 (m, 1H), 1.83−1.55 (m, 2H). LCMS (ESI): m/z= 336.5 $(M+H)^+$.

Synthesis of 4-(4-(((1-(Hydroxymethyl)cyclopentyl)methyl)-amino)-7H-pyrrolo[2,3-d]pyrimidin-6-yl)-1-methyl-1H-pyrazole-5-carbonitrile (AVI-6254). To a solution of 4-(4-chloro-7-((2-(trimethylsilyl)ethoxy)methyl)-7H-pyrrolo[2,3-*d*]pyrimidin-6-yl)-1-methyl-1H-pyrazole-5-carbonitrile (100.0 mg, 0.25 mmol) in DMSO (2 mL) was added (1-(aminomethyl)cyclopentyl)methanol (49.9 mg, 0.38 mmol) and TEA (52.1 mg, 0.51 mmol). After stirred at 100 °C for 1 h, the reaction mixture was extracted with ethyl acetate (3 × 20 mL), washed with brine (10 mL) and dried over Na_2SO_4. The organic layers were concentrated and the residue was purified by silica gel chromatography (DCM/MeOH, 20:1) to obtain 4-(4-(((1-(hydroxymethyl)cyclopentyl)methyl)amino)-7-((2-(trimethylsilyl)-ethoxy)methyl)-7H-pyrrolo[2,3-*d*]pyrimidin-6-yl)-1-methyl-1H-pyrazole-5-carbonitrile as a yellow solid (120 mg, Yield: 97%). LCMS (ESI): m/z = 482.4 $(M+H)^+$.

To a solution of the above intermediate (120 mg, 0.25 mmol) in DCM (2 mL) was added TFA (1.0 mL). After stirring at 20 °C for 3 h, the reaction mixture was concentrated to dryness. To the resulting residue was added saturated aqueous NaHCO3 (5 mL) and extracted with DCM (30 mL × 2). The organic layers were washed with brine and concentrated under reduced pressure. The crude was purified by prep-HPLC (10−50% 0.1% NH_4HCO_3 in water/ACN) to obtain **AVI-6254** as a white solid (29 mg, Yield: 33.33%). 1H NMR (500 MHz, DMSO-d6) δ 12.19 (s, 1H), 8.12 (d, J = 12.0 Hz, 2H), 7.85 (s, 1H), 7.11 (s, 1H), 5.41 (s, 1H), 4.05 (s, 3H), 3.44 (d, J = 6.4 Hz, 2H), 3.14 (d, J = 6.6 Hz, 2H), 1.58 (dd, J = 17.5, 6.9 Hz, 4H), 1.49−1.43 (m, 2H), 1.40−1.34 (m, 2H). LCMS (ESI): m/z= 352.4 $(M+H)^+$.

Synthesis of 4-(4-(((3,3-Difluoro-1-(hydroxymethyl)cyclobutyl)-methyl)amino)-7H-pyrrolo[2,3-d]pyrimidin-6-yl)-1-methyl-1H-pyrazole-5-carbonitrile (AVI-6253). To a solution of 4-(4-chloro-7-((2-

https://doi.org/10.1021/acs.jmedchem.5c02933
J. Med. Chem. XXXX, XXX, XXX−XXX

(trimethylsilyl)ethoxy)methyl)-7H-pyrrolo[2,3-*d*]pyrimidin-6-yl)-1-methyl-1H-pyrazole-5-carbonitrile (120 mg, 0.31 mmol) in dry DMSO (5 mL) was added (1-(aminomethyl)-3,3-difluorocyclobutyl)-methanol (70 mg, 0.46 mmol) and TEA (156 mg, 1.55 mmol). After stirring at 110 °C for 3 h, the reaction mixture was diluted with ethyl acetate (50.0 mL), washed with water (10.0 mL) and brine (10.0 mL). The organic layer was dried over Na_2SO_4 and concentrated under reduced pressure. The residue was purified by column chromatography on silica gel (DCM/MeOH, 10:1)) to obtain 4-(4-(((3,3-difluoro-1-(hydroxymethyl)cyclobutyl)methyl)amino)-7-((2-(trimethylsilyl)ethoxy)methyl)-7H-pyrrolo[2,3-*d*]pyrimidin-6-yl)-1-methyl-1H-pyrazole-5-carbonitrile (100 mg, Yield: 64.3%) as a white solid. LCMS (ESI): m/z = 504.3 $(M+H)^+$.

To a solution of the above intermediate (100 mg, 0.2 mmol) in DCM (3 mL) was added TFA (1 mL). After stirring at 20 °C for 4 h, the reaction mixture was concentrated to dryness. To the resulting residue was added saturated aqueous NaHCO3 (5 mL) and extracted with DCM (30 mL × 2). The organic layers were washed with brine and concentrated under reduced pressure. The crude was purified by prep-HPLC (10−100% 10 mmol NH_4HCO_3 in water/ACN) to obtain **AVI-6253** as a white solid (27 mg, yield: 36.4%).

Synthesis of 4-(4-((3-Hydroxy-2,2-dimethylpropyl)amino)-7H-pyrrolo[2,3-d]pyrimidin-6-yl)-1-methyl-1H-pyrazole-5-carbonitrile (AVI-6252). To a solution of 4-(4-chloro-7-((2-(trimethylsilyl)-ethoxy)methyl)-7H-pyrrolo[2,3-*d*]pyrimidin-6-yl)-1-methyl-1H-pyrazole-5-carbonitrile (200 mg, 0.52 mmol) in DMSO (2 mL) was added 3-amino-2,2-dimethylpropan-1-ol (77 mg, 0.75 mmol) and TEA (158 mg, 1.56 mmol). After stirring at 100 °C for 4 h, the reaction mixture was diluted with dichloromethane (5 mL) and washed with water (10.0 mL × 3). The organic layer was dried over Na_2SO_4 and concentrated under reduced pressure. The residue was purified by silica gel chromatography (DCM/MeOH, 10:1) to obtain 4-(4-((3-hydroxy-2,2-dimethylpropyl)amino)-7-((2-(trimethylsilyl)ethoxy)-methyl)-7H-pyrrolo[2,3-*d*]pyrimidin-6-yl)-1-methyl-1H-pyrazole-5-carbonitrile (90 mg, Yield: 38.0%) as a white solid. LCMS (ESI): m/z = 456.2 $(M+H)^+$.

To a solution of the above intermediate (90 mg, 0.20 mmol) in DCM (2.0 mL) was added TFA (0.5 mL). After stirring at 20 °C for 4 h, the reaction mixture was concentrated to dryness. To the resulting residue was added saturated aqueous $NaHCO_3$ (5 mL) and extracted with DCM (30 mL × 2). The organic layers were washed with brine and concentrated under reduced pressure. The crude was purified by prep-HPLC (10−50% 0.1% NH_4HCO_3 in water/MeCN) to obtain **AVI-6252** as a white solid (29 mg, yield: 44.6%). ^{1}H NMR (500 MHz, DMSO) δ 12.19 (s, 1H), 8.12 (d, J = 11.9 Hz, 2H), 7.83 (s, 1H), 7.14 (d, J = 1.4 Hz, 1H), 5.27 (s, 1H), 4.05 (s, 3H), 3.34 (d, J = 6.4 Hz, 2H), 3.07 (s, 2H), 0.87 (s, 6H). LCMS (ESI): m/z= 325.3 $(M+H)^+$.

Synthesis of 1-(4-((2,2-Dimethyl-5-oxopyrrolidin-1-yl)amino)-9H-pyrimido[4,5-b]indol-8-yl)-3-ethylurea (AVI-6347). To a solution of 1-(4-chloro-9H-pyrimido[4,5-*b*]indol-8-yl)-3-ethylurea (100 mg, 0.35 mmol) in dry DMSO (3.0 mL) was added 3-amino-4,4-dimethyloxazolidin-2-one (67 mg, 0.52 mmol), $Pd_2(dba)_3$ (32 mg, 0.03 mmol), tri*tert*-butylphosphine tetrafluoroborate (15 mg, 0.05 mmol) and *t*-BuONa(83 mg, 0.86 mmol). After stirring at 100 °C for 2 h, the reaction mixture was filtered and the filtrate was purified by reversed phase chromatography (10−32% acetonitrile/water/0.1% TFA). Further purification by silica gel column chromatography (dichloromethane/methanol 10:1) afforded **AVI-6347** (20 mg, yield: 15%) as a white solid. ^{1}H NMR (500 MHz, DMSO-*d6*) δ 11.74 (s, 1H), 9.28 (s, 1H), 8.45 (d, J = 10.6 Hz, 1H), 8.38 (s, 1H), 8.07 (d, J = 7.8 Hz, 1H), 7.61 (d, J = 7.8 Hz, 1H), 7.22 (t, J = 7.9 Hz, 1H), 6.29 (t, J = 5.5 Hz, 1H), 4.29 (s, 2H), 3.22−3.16 (m, 2H), 1.34 (s, 6H), 1.11 (t, J = 7.2 Hz, 3H). LCMS (ESI): m/z = 384.3 $(M+H)^+$.

Synthesis of 1-(4-((2,2-Dimethyl-5-oxopyrrolidin-1-yl)amino)-9H-pyrimido[4,5-b]indol-8-yl)-3-(2-methoxyethyl)urea (AVI-6187). To a solution of 1-((8-amino-9H-pyrido[2,3-*b*]indol-4-yl)amino)-5,5-dimethylpyrrolidin-2-one (20 mg, 0.064 mmol) and triethylamine (0.026 mL, 0.26 mmol) in THF (1 mL), was added 1-isocyanato-2-methoxyethane (0.013 mg, 0.13 mmol). After stirring at 55 °C for 18 h, the reaction mixture was purified by reverse phase chromatography (water/acetonitrile) to obtain **AVI-6187** as a white solid (4.3 mg; Yield: 16%). 1H NMR (METHANOL-d4, 400 MHz) δ 8.27 (s, 1H), 7.86 (d, 1H, J = 8.0 Hz), 7.29 (d, 1H, J = 7.8 Hz), 7.14 (t, 1H, J = 7.5 Hz), 3.57−3.60 (m, 2H), 3.49−3.51 (m, 2H), 3.44 (s, 3H), 2.61 (t, 2H, J = 8.0 Hz), 2.21 (br s, 2H), 1.37 (s, 6H). LCMS (ESI): m/z= 412 $(M+H)^+$.

Synthesis of 1-(4-((2,2-Dimethyl-5-oxopyrrolidin-1-yl)amino)-9H-pyrimido[4,5-b]indol-8-yl)-3-(tetrahydro-2H-pyran-4-yl)urea (AVI-6188). To a solution of 1-((8-amino-9H-pyrido[2,3-*b*]indol-4-yl)amino)-5,5-dimethylpyrrolidin-2-one (20 mg, 0.064 mmol) and triethylamine (0.026 mL, 0.26 mmol) in THF (1 mL), was added 4-isocyanatotetrahydro-2H-pyran (0.016 mg, 0.13 mmol). After stirring at 55 °C for 18 h, the reaction mixture was purified by reverse phase chromatography (water/acetonitrile) to obtain **AVI-6188** as a white solid (3.6 mg; Yield: 13%). ^{1}H NMR (METHANOL-d_4, 400 MHz) δ 8.33 (s, 1H), 7.94 (dd, 1H, J = 1.0, 7.8 Hz), 7.32 (dd, 1H, J = 0.7, 7.8 Hz), 7.23 (t, 1H, J = 7.8 Hz), 3.88−4.01 (m, 3H), 3.52−3.59 (m, 2H), 2.60 (t, 2H, J = 7.9 Hz), 2.20 (br s, 2H), 1.98 (br d, 2H, J = 2.2 Hz), 1.60 (br s, 2H), 1.39 (s, 6H). LCMS (ESI): m/z = 438 $(M+H)^+$.

Synthesis of 5,5-Dimethyl-1-((8-(trifluoromethyl)-9H-pyrimido-[4,5-b]indol-4-yl)amino)pyrrolidin-2-one (AVI-6371). To a solution of 4-chloro-8-(trifluoromethyl)-9H-pyrimido[4,5-*b*]indole (200 mg, 0.74 mmol) in dry DMSO (4 mL) was added 1-amino-5,5-dimethylpyrrolidin-2-one (142 mg, 1.1 mmol) and *t*-BuOK (414 mg, 3.69 mmol). The mixture was stirred at 100 °C for 45 min, diluted with ethyl acetate (50.0 mL) and washed with water (10.0 mL), brine (10.0 mL). The organic layers was dried over Na_2SO_4 and concentrated under reduced pressure. The residue was purified by reverse phase chromatography (10 mM NH_4HCO_3 in water, 5−60% ACN) to give **AVI-6371** as a white solid (25 mg, yield: 9.33%). ^{1}H NMR (500 MHz, DMSO-*d6*) δ 12.57 (s, 1H), 9.33 (s, 1H), 8.73 (d, J = 7.8 Hz, 1H), 8.49 (s, 1H), 7.77 (d, J = 7.7 Hz, 1H), 7.48 (t, J = 7.8 Hz, 1H), 2.45 (t, J = 7.8 Hz, 2H), 2.04 (t, J = 7.7 Hz, 2H), 1.30 (s, 6H). LCMS (ESI): m/z = 364.3 $(M+H)^+$.

Synthesis of 4,4-Dimethyl-3-((8-(trifluoromethyl)-9H-pyrimido-[4,5-b]indol-4-yl)amino)oxazolidin-2-one (AVI-6372). To a solution of 4-chloro-8-(trifluoromethyl)-9H-pyrimido[4,5-*b*]indole (50 mg, 0.18 mmol) and 3-amino-4,4-dimethyloxazolidin-2-one (36 mg, 0.27 mmol) in i-PrOH (0.8 mL) was added 1N aqueous HCl (0.2 mL). The reaction mixture was stirred at 100 °C for 18 h, concentrated and the residue was purified by reverse phase chromatography (water/10−100% MeCN) to obtain 2.1 mg (3%) of **AVI-6372** as a white colored solid (2.1 mg; Yield: 3%). 1H NMR (METHANOL-d4, 400 MHz) δ 8.50−8.57 (m, 2H), 7.79 (d, 1H, J = 7.8 Hz), 7.49 (t, 1H, J = 7.8 Hz), 4.41 (br s, 2H), 1.47 (br s, 6H). LCMS (ESI): m/z = 366 $(M+H)^+$.

Synthesis of 5,5-Dimethyl-1-((8-methyl-9H-pyrimido[4,5-b]indol-4-yl)amino)pyrrolidin-2-one (AVI-6355). To a solution of 8-bromo-4-chloro-9H-pyrimido[4,5-*b*]indole (4 g, 14.23 mmol) in dry DMSO (50 mL) was added 1-amino-5,5-dimethylpyrrolidin-2-one (2.73 g, 21.35 mmol) and *t*-BuOK (3.99 g, 35.58 mmol). The mixture was stirred at 100 °C for 45 min, diluted with ethyl acetate (80.0 mL) and washed with water (100.0 mL), brine (100.0 mL). The organic layers were dried over Na_2SO_4 and concentrated under reduced pressure. The crude product was purified by silica gel chromatography (dichloromethane/methanol 10:1) to obtain 1-((8-bromo-9H-pyrimido[4,5-*b*]indol-4-yl)amino)-5,5-dimethylpyrrolidin-2-one as a brown solid (2 g, yield: 37.66%). ^{1}H NMR (500 MHz, DMSO) δ 12.65 (s, 1H), 9.55 (br s, 1H), 8.50 (s, 1H), 8.46 (d, J = 7.8 Hz, 1H), 7.69 (d, J = 7.7 Hz, 1H), 7.29 (t, J = 7.9 Hz, 1H), 2.45 (t, J = 7.9 Hz, 2H), 2.05 (t, J = 7.8 Hz, 2H), 1.29 (s, 6H). LCMS (ESI): m/z = 374.1 $(M+H)^+$.

To a solution of the above intermediate (120 mg, 0.32 mmol) in dioxane (2 mL) and H_2O (0.2 mL) was added methylboronic acid (38 mg, 0.64 mmol), K_2CO_3 (110 mg, 0.80 mmol) and $Pd(dppf)Cl_2$ (35 mg, 0.05 mmol). The mixture was stirred at 95 °C for 16 h under N_2. The reaction mixture was diluted with water (50 mL) and extracted with DCM (3 × 50 mL). The organic layer was dried over Na_2SO_4 and concentrated under reduced pressure. The residue was

https://doi.org/10.1021/acs.jmedchem.5c02933
J. Med. Chem. XXXX, XXX, XXX−XXX

purified by reverse phase chromatography (10 mM NH_4HCO_3 in water, 5−35% MeCN) to obtain **AVI-6355** as a white solid (25 mg, yield: 14.63%). ^{1}H NMR (500 MHz, DMSO-*d6*) δ 12.08 (s, 1H), 9.05 (s, 1H), 8.39 (s, 1H), 8.23 (t, J = 16.0 Hz, 1H), 7.32−7.10 (m, 2H), 2.56 (s, 3H), 2.42 (t, J = 7.8 Hz, 2H), 2.03 (t, J = 7.8 Hz, 2H), 1.27 (d, J = 21.2 Hz, 6H). LCMS (ESI): m/z = 310.4 $(M+H)^+$.

Synthesis of 4,4-Dimethyl-3-((8-methyl-9H-pyrimido[4,5-b]indol-4-yl)amino)oxazolidin-2-one (AVI-6357). To a solution of 4-chloro-8-methyl-9H-pyrimido[4,5-*b*]indole(50 mg, 0.23 mmol) and 3-amino-4,4-dimethyloxazolidin-2-one (45 mg, 0.34 mmol) in i-PrOH (0.8 mL) was added 1N aqueous HCl (0.2 mL). The reaction mixture was stirred at 100 °C for 18 h, concentrated and the residue was purified by reverse phase chromatography (water/10−100% MeCN) to obtain **AVI-6357** (18 mg, Yield: 25%) as a cream colored solid. ^{1}H NMR (DMSO-d_6, 400 MHz) δ 12.15 (s, 1H), 9.27 (s, 1H), 8.46 (s, 1H), 8.24 (br d, 1H, J = 7.3 Hz), 7.22−7.27 (m, 2H), 4.29 (s, 2H), 2.57 (s, 3H), 1.35 (br s, 6H). LCMS (ESI): m/z = 312 $(M+H)^+$.

Synthesis of 1-((8-Cyclopropyl-9H-pyrimido[4,5-b]indol-4-yl)-amino)-5,5-dimethylpyrrolidin-2-one (AVI-6354). To a solution of 1-((8-bromo-9H-pyrimido[4,5-*b*]indol-4-yl)amino)-5,5-dimethylpyrrolidin-2-one (200 mg, 0.53 mmol) in dioxane (5 mL) and water (0.5 mL) was added cyclopropylboronic acid (184 mg, 2.14 mmol), K_2CO_3 (185 mg, 1.34 mmol) and $Pd(dppf)Cl_2$ (58 mg, 0.08 mmol). The mixture was stirred at 95 °C for 16 h under N_2. The reaction mixture was then diluted with water (50 mL) and extracted with DCM (3 × 50 mL). The organic layers were dried over Na_2SO_4 and concentrated under reduced pressure. The residue was purified by reverse phase chromatography (10 mM NH_4HCO_3 in water, 5−50% ACN) to give **AVI-6354** as a white solid (25 mg, yield: 13.91%). ^{1}H NMR (500 MHz, DMSO-*d6*) δ 12.22 (s, 1H), 9.05 (s, 1H), 8.40 (s, 1H), 8.22 (d, J = 7.8 Hz, 1H), 7.19 (t, J = 7.7 Hz, 1H), 6.97 (d, J = 7.5 Hz, 1H), 2.43−2.39 (m, 3H), 2.03 (t, J = 7.8 Hz, 2H), 1.29 (s, 6H), 1.08 − 1.02 (m, 2H), 0.80 − 0.75 (m, 2H). LCMS (ESI): m/z = 336.3 $(M+H)^+$.

Synthesis of 4,4-Dimethyl-3-((8-(cyclopropyl)-9H-pyrimido[4,5-b]indol-4-yl)amino)oxazolidin-2-one (AVI-6373). To a solution of 4-chloro-8-(cyclopropyl)-9H-pyrimido[4,5-*b*]indole (50 mg, 0.21 mmol) and 3-amino-4,4-dimethyloxazolidin-2-one (40 mg, 0.31 mmol) in i-PrOH (0.8 mL) was added 1N aqueous HCl (0.2 mL). The reaction mixture was stirred at100 °C for 18 h, concentrated and the residue was purified by reverse phase chromatography (water/10−100% MeCN) to obtain of **AVI-6373** as a white colored solid (2.2 mg; Yield: 3%). ^{1}H NMR (METHANOL-d_4, 400 MHz) δ 8.45 (s, 1H), 8.05 (d, 1H, J = 7.8 Hz), 7.27 (t, 1H, J = 7.7 Hz), 7.12 (d, 1H, J = 7.3 Hz), 4.40 (br s, 2H), 2.28−2.35 (m, 1H), 1.45 (br s, 6H), 1.12 (dd, 2H, J = 1.8, 8.4 Hz), 0.83 (dd, 2H, J = 1.7, 5.1 Hz). LCMS (ESI): m/z = 338 $(M+H)^+$.

Synthesis of 5,5-Dimethyl-1-((6-(trifluoromethyl)-9H-pyrimido-[4,5-b]indol-4-yl)amino)pyrrolidin-2-one (AVI-3769). A solution of 4-chloro-6-(trifluoromethyl)-9H-pyrimido[4,5-*b*]indole (900 mg, 3.3 mmol) and 1-amino-5,5-dimethylpyrrolidin-2-one hydrochloride (637.6 mg, 4.98 mmol,) in isopropanol (10 mL) and concentrated HCl (1 drop) was stirred at 100 °C for 16 h. The reaction mixture was concentrated under reduced pressure and the residue was purified by reverse phase chromatography ((0.1% NH_4HCO_3 in water, 10−100%ACN) to obtain of **AVI-3769** as a white solid (102 mg; Yield: 9.9%). 1H NMR (500 MHz, DMSO) δ 12.55 (s, 1H), 9.47 (s, 1H), 8.93 (s, 1H), 8.46 (s, 1H), 7.75 (d, 1H, J = 8.5 Hz), 7.68 (d, 1H, J = 8.5 Hz), 2.45 (t, 2H, J = 7.8 Hz), 2.04 (d, 2H, J = 7.5 Hz), 1.30 (s, 6H). LCMS (ESI): m/z 364 $(M+H)^+$.

Synthesis of 4,4-Dimethyl-3-((6-(trifluoromethyl)-9H-pyrimido-[4,5-b]indol-4-yl)amino)oxazolidin-2-one (AVI-6412). To a solution of 4-chloro-6-(trifluoromethyl)-9H-pyrimido[4,5-*b*]indole (50 mg, 0.18 mmol) and 3-amino-4,4-dimethyloxazolidin-2-one (36 mg, 0.27 mmol) in i-PrOH (0.8 mL) was added 1N aqueous HCl (0.2 mL). The reaction mixture was stirred at 100 °C for 18 h, concentrated and the residue was purified by reverse phase chromatography (water/10−100% MeCN) to obtain of **AVI-6412** as a white colored solid (6 mg; Yield: 9%). ^{1}H NMR (METHANOL-d_4, 400 MHz) δ 8.68 (s, 1H), 8.47 (s, 1H), 7.69−7.77 (m, 2H), 4.41 (br s, 2H), 1.46 (br s, 6H). LCMS (ESI): m/z = 366 $(M+H)^+$.

Synthesis of 1-((6-Cyclopropyl-9H-pyrimido[4,5-b]indol-4-yl)-amino)-5,5-dimethylpyrrolidin-2-one (AVI-3865). A neat mixture of 4-chloro-6-cyclopropyl-9H-pyrimido[4,5-*b*]indole (260 mg, 1.07 mmol) and 1-amino-5,5-dimethylpyrrolidin-2-one hydrochloride (351 mg, 2.14 mmol) was heated at 115 °C for 16 h. The reaction mixture was taken in water (10 mL) and extracted with ethyl acetate (3 × 20 mL). The organic layer was dried over Na_2SO_4 and concentrated. The residue was purified by reverse phase chromatography (0.1% NH_4HCO_3 in water/MeCN) to obtain of **AVI-3865** as a white solid (26 mg; Yield: 7.3%). ^{1}H NMR (500 MHz, DMSO) δ 11.94 (s, 1H), 9.10 (s, 1H), 8.34 (s, 1H), 8.08 (s, 1H), 7.38 (d, J = 8.3 Hz, 1H), 7.20 (d, J = 8.3 Hz, 1H), 2.47−2.35 (m, 2H), 2.06 (ddd, J = 16.3, 11.1, 6.6 Hz, 3H), 1.27 (d, J = 19.4 Hz, 6H), 1.01−0.93 (m, 2H), 0.85−0.74 (m, 2H). LCMS (ESI): m/z = 336 $(M+H)^+$.

Synthesis of 3-((8-Cyclopropyl-6-fluoro-9H-pyrimido[4,5-b]indol-4-yl)amino)-4,4-dimethyloxazolidin-2-one (AVI-6451). To a solution of 4-chloro-8-cyclopropyl-6-fluoro-9H-pyrimido[4,5-*b*]indole (900 mg, 3.45 mmol) in i-PrOH (20 mL) was added 3-amino-4,4-dimethyloxazolidin-2-one (897 mg, 6.9 mmol) and conc. HCl (0.1 mL). After stirring at 100 °C for 72 h, the reaction mixture was concentrated and the residue was purified by reverse phase chromatography (0.1% NH4HCO_3 in water, 10−100%ACN) to obtain **AVI-6451** as a white solid (220 mg, Yield: 17.9%). 1H NMR (500 MHz, DMSO-d6) δ 12.39 (s, 1H), 9.31 (s, 1H), 8.47 (s, 1H), 8.13 (d, J = 8.2 Hz, 1H), 6.84 (dd, J = 10.8, 2.2 Hz, 1H), 4.29 (s, 2H), 2.48 − 2.42 (m, 1H), 1.46 − 1.27 (m, 6H), 1.09 (dd, J = 8.3, 1.7 Hz, 2H), 0.85 (d, J = 4.1 Hz, 2H). LCMS (ESI): m/z 356.1 $(M+H)^+$.

Synthesis of 3-((8-Cyclopropyl-7-fluoro-9H-pyrimido[4,5-b]indol-4-yl)amino)-4,4-dimethyloxazolidin-2-one (AVI-6452). To a solution of 4-chloro-8-cyclopropyl-7-fluoro-9H-pyrimido[4,5-*b*]indole (900 mg, 3.45 mmol) in isopropanol (20 mL) was added 3-amino-4,4-dimethyloxazolidin-2-one (897 mg, 6.9 mmol) and conc. HCl (0.1 mL). The mixture was stirred at 100 °C for 72 h, concentrated under reduced pressure and the residue was purified by reverse phase chromatography (0.1% NH_4HCO_3 in water, 10−100% MeCN) to obtain **AVI-6452** as a white solid (240 mg, yield: 19.6%). ^{1}H NMR (400 MHz, DMSO) δ 12.31 (s, 1H), 9.32 (s, 1H), 8.46 (s, 1H), 8.24 (dt, J = 13.8, 6.9 Hz, 1H), 7.10 (dd, J = 11.7, 8.7 Hz, 1H), 4.29 (s, 2H), 2.08 (tt, J = 8.6, 5.4 Hz, 1H), 1.30 (t, J = 26.8 Hz, 6H), 1.18 − 0.98 (m, 2H), 0.92 − 0.76 (m, 2H). LCMS (ESI): m/z 356.2 $(M+H)^+$.

Synthesis of 3-((6-Fluoro-8-(1-hydroxycyclopropyl)-9H-pyrimido-[4,5-b]indol-4-yl)amino)-4,4-dimethyloxazolidin-2-one (AVI-6612). To solution of (4-chloro-6-fluoro-9H-pyrimido[4,5-*b*]indol-8-yl)-cyclopropan-1-ol (100 mg, 0.36 mmol) in *i*-PrOH (6 mL) was added 3-amino-4,4-dimethyloxazolidin-2-one (94 mg, 0.72 mmol) and conc. HCl (0.1 mL). After stirring at 100 °C for 16 h, the reaction mixture was concentrated and the residue was purified by reverse phase chromatography (10 mmol NH_4HCO_3 in water, 10−100% ACN) to obtain **AVI-6612** as a white solid (15 mg, yield: 11.2%). ^{1}H NMR (400 MHz, DMSO) δ 11.73 (d, J = 24.3 Hz, 1H), 9.36 (s, 1H), 8.49 (s, 1H), 8.25 (dd, J = 9.7, 1.9 Hz, 1H), 7.15 (dd, J = 10.2, 2.4 Hz, 1H), 6.10 (d, J = 5.1 Hz, 1H), 4.29 (s, 2H), 1.30 (dd, J = 31.3, 27.0 Hz, 6H), 1.14 (d, J = 13.9 Hz, 2H), 1.08 − 0.89 (m, 2H). LCMS (ESI): m/z 372.1 $(M+H)^+$.

Synthesis of 3-((6-Fluoro-8-(1-fluorocyclopropyl)-9H-pyrimido-[4,5-b]indol-4-yl)amino)-4,4-dimethyloxazolidin-2-one (AVI-6613). To a solution of 1-(4-chloro-6-fluoro-9H-pyrimido[4,5-*b*]indol-8-yl)cyclopropan-1-ol (200 mg, 0.72 mmol) in dichloromethane (10 mL) was added DAST (581 mg, 3.61 mmol) and the mixture was stirred at room temperature for an hour under nitrogen gas. The mixture was then quenched with saturated aqueous $NaHCO_3$. The layers were separated and aqueous layer was extracted with ethyl acetate (3 × 30 mL), The combined organic layers were dried over anhydrous Na_2SO_4, filtered and concentrated under reduced pressure. The crude residue was then purified by silica gel chromatography (3:1 petroleum ether/ethyl acetate) to afford 4-chloro-6-fluoro-8-(1-

https://doi.org/10.1021/acs.jmedchem.5c02933
J. Med. Chem. XXXX, XXX, XXX−XXX

fluorocyclopropyl)-9H-pyrimido[4,5-*b*]indole as a white solid (150 mg, Yield: 74.5%). LCMS (ESI): m/z = 280.2 $(M+H)^+$.

To solution of the above intermediate (100 mg, 0.36 mmol) in *i*-PrOH (6 mL) was added 3-amino-4,4-dimethyloxazolidin-2-one (94 mg, 0.72 mmol) and conc. HCl (0.1 mL). The mixture was stirred at 100 °C for 16 h, concentrated and the residue was purified by reverse phase chromatography (10 mmol NH_4HCO_3 in water, 10−100% ACN) to obtain **AVI-6613** as a white solid (13 mg, yield: 9.76%). ^{1}H NMR (400 MHz, DMSO) δ 12.41 (d, J = 36.2 Hz, 1H), 9.42 (s, 1H), 8.51 (s, 1H), 8.42 (d, J = 9.5 Hz, 1H), 7.40 (d, J = 9.7 Hz, 1H), 4.30 (s, 2H), 1.55 (d, J = 18.6 Hz, 2H), 1.34 (d, J = 33.5 Hz, 6H), 1.20 (t, J = 15.1 Hz, 2H). LCMS (ESI): m/z 374.2 $(M+H)^+$.

■ ASSOCIATED CONTENT

Supporting Information

The Supporting Information is available free of charge at https://pubs.acs.org/doi/10.1021/acs.jmedchem.5c02933.

Molecular formula strings and properties (CSV)
Dose−response curves from HTRF assay; plasma exposure profile curves for AVI-6451; plasma exposure profile curves for AVI-6452; tables of PK data and parameters for AVI-6451; tables of PK data and parameters for AVI-6452; tables of crystallographic data collection and refinement statistics; representative HPLC chromatographs for key analogs; supplementary experimental procedures; and supplementary synthetic schemes and procedures (PDF)
avi4206 (PDB)
avi-6451 (PDB)

■ AUTHOR INFORMATION

Corresponding Authors

James S. Fraser − *Department of Bioengineering and Therapeutic Sciences, University of California, San Francisco, San Francisco, California 94158, United States;* orcid.org/0000-0002-5080-2859; Email: jfraser@fraserlab.com

Adam R. Renslo − *Department of Pharmaceutical Chemistry, University of California, San Francisco, San Francisco, California 94158, United States; Helen Diller Family Comprehensive Cancer Center, University of California, San Francisco, San Francisco, California 94158, United States;* orcid.org/0000-0002-1240-2846; Email: adam.renslo@ucsf.edu

Authors

Priyadarshini Jaishankar − *Department of Pharmaceutical Chemistry, University of California, San Francisco, San Francisco, California 94158, United States*

Galen J. Correy − *Department of Bioengineering and Therapeutic Sciences, University of California, San Francisco, San Francisco, California 94158, United States*

Yusuke Matsui − *Gladstone Institute of Virology, Gladstone Institutes, San Francisco, California 94158, United States*

Takaya Togo − *Department of Pharmaceutical Chemistry, University of California, San Francisco, San Francisco, California 94158, United States*

Moira M. Rachman − *Department of Pharmaceutical Chemistry, University of California, San Francisco, San Francisco, California 94158, United States;* orcid.org/0000-0003-3671-8885

Maisie G.V. Stevens − *Helen Diller Family Comprehensive Cancer Center, University of California, San Francisco, San Francisco, California 94158, United States*

Eric R. Hantz − *Department of Pharmaceutical Chemistry, University of California, San Francisco, San Francisco, California 94158, United States;* orcid.org/0000-0002-2588-7619

Jeffrey Zheng − *Department of Pharmaceutical Chemistry, University of California, San Francisco, San Francisco, California 94158, United States;* orcid.org/0000-0002-4691-9317

Morgan E. Diolaiti − *Helen Diller Family Comprehensive Cancer Center, University of California, San Francisco, San Francisco, California 94158, United States;* orcid.org/0000-0001-5900-3060

Mauricio Montano − *Gladstone Institute of Virology, Gladstone Institutes, San Francisco, California 94158, United States*

Taha Y. Taha − *Gladstone Institute of Virology, Gladstone Institutes, San Francisco, California 94158, United States;* orcid.org/0000-0002-7344-7490

Julia Rosecrans − *Gladstone Institute of Virology, Gladstone Institutes, San Francisco, California 94158, United States*

Julius Pampel − *Department of Bioengineering and Therapeutic Sciences, University of California, San Francisco, San Francisco, California 94158, United States*

Nevan J. Krogan − *Department of Bioengineering and Therapeutic Sciences, University of California, San Francisco, San Francisco, California 94158, United States;* orcid.org/0000-0003-4902-337X

Brian K. Shoichet − *Department of Pharmaceutical Chemistry, University of California, San Francisco, San Francisco, California 94158, United States;* orcid.org/0000-0002-6098-7367

Alan Ashworth − *Helen Diller Family Comprehensive Cancer Center, University of California, San Francisco, San Francisco, California 94158, United States*

Melanie Ott − *Gladstone Institute of Virology, Gladstone Institutes, San Francisco, California 94158, United States*

Complete contact information is available at: https://pubs.acs.org/10.1021/acs.jmedchem.5c02933

Author Contributions

⊥P.J., G.J.C., Y.M, and T.T. contributed equally to this work.

Notes

The authors declare the following competing financial interest(s): P.J., G.J.C., T.T., M.M.R., E.R.H., M.D., N.J.K., B.K.S, A.A, M.O., J.S.F, and A.R.R. are listed as inventors on a patent application describing compounds described herein. M.O. and T.Y.T. are listed as inventors on a patent filed by the Gladstone Institutes that covers the use of pGLUE to generate SARS-CoV-2 infectious clones and replicons.

■ ACKNOWLEDGMENTS

This work was supported by the National Institutes of Health NIAID Antiviral Drug Discovery (AViDD) grant U19AI171110. M.O. received support from the Roddenberry Foundation, from P. and E. Taft, and the Gladstone Institutes. M.O. is a Chan Zuckerberg Biohub − San Francisco Investigator. The ALS, a U.S. DOE Office of Science User Facility under contract no. DE-AC02-05CH11231, is supported in part by the ALS-ENABLE program funded by the NIH, National Institute of General Medical Sciences, grant P30 GM124169. Use of the SSRL, SLAC National Accelerator Laboratory, is supported by the U.S. Department of Energy,

https://doi.org/10.1021/acs.jmedchem.5c02933
J. Med. Chem. XXXX, XXX, XXX−XXX

Office of Science, Office of Basic Energy Sciences under Contract No. DE-AC02-76SF00515. The SSRL Structural Molecular Biology Program is supported by the DOE Office of Biological and Environmental Research, and by the National Institutes of Health, National Institute of General Medical Sciences (P30GM133894).Portions of this work were performed on the Wynton HPC Co-Op cluster, which is supported by UCSF research faculty and UCSF institutional funds. The authors wish to thank the UCSF Wynton team for their ongoing technical support of the Wynton environment.

■ ABBREVIATIONS

hACE2, human angiotensin converting enzyme 2; ADME, absorption, distribution, metabolism, and excretion; BID, twice daily; CoV, coronavirus; CYP, cytochrome; DCM, dichloromethane; DFT, density functional theory; ER, efflux ratio; HP-βCD, hydroxypropyl-β-cyclodextrin; HPMC, (hydroxypropyl)-methyl cellulose; HTRF, homogeneous time-resolved fluorescence; IFN-γ, interferon gamma; IP, intraperitoneal; ITC, isothermal titration calorimetry; M-CSF, macrophage colony-stimulating factor; MDM, monocyte-derived macrophages; MLM, mouse liver microsomes; PARP, poly(ADP-ribose) polymerase; PBMC, peripheral blood mononuclear cells; PBS, phosphate buffered saline; PD, pharmacodynamic; PFU, plaque forming units; P-gp, P-glycoprotein; PK, pharmacokinetic; PO, orally administered; QD, once daily; TMPRSS2, transmembrane protease, serine 2

■ REFERENCES

(1) Li, G.; Hilgenfeld, R.; Whitley, R.; De Clercq, E. Therapeutic Strategies for COVID-19: Progress and Lessons Learned. *Nat. Rev. Drug Discovery* **2023**, *22*, 449−475.

(2) von Delft, A.; Hall, M. D.; Kwong, A. D.; Purcell, L. A.; Saikatendu, K. S.; Schmitz, U.; Tallarico, J. A.; Lee, A. A. Accelerating Antiviral Drug Discovery: Lessons from COVID-19. *Nat. Rev. Drug Discovery* **2023**, *22*, 585−603.

(3) Leung, A. K. L.; Griffin, D. E.; Bosch, J.; Fehr, A. R. The Conserved Macrodomain Is a Potential Therapeutic Target for Coronaviruses and Alphaviruses. *Pathogens* **2022**, *11*, 94.

(4) Alhammad, Y. M.; Parthasarathy, S.; Ghimire, R.; Kerr, C. M.; O'Connor, J. J.; Pfannenstiel, J. J.; Chanda, D.; Miller, C. A.; Baumlin, N.; Salathe, M.; Unckless, R. L.; Zuñiga, S.; Enjuanes, L.; More, S.; Channappanavar, R.; Fehr, A. R. SARS-CoV-2 Mac1 Is Required for IFN Antagonism and Efficient Virus Replication in Cell Culture and in Mice. *Proc. Natl. Acad. Sci. U. S. A.* **2023**, *120*, No. e2302083120.

(5) Taha, T. Y.; Suryawanshi, R. K.; Chen, I. P.; Correy, G. J.; McCavitt-Malvido, M.; O'Leary, P. C.; Jogalekar, M. P.; Diolaiti, M. E.; Kimmerly, G. R.; Tsou, C.-L.; Gascon, R.; Montano, M.; Martinez-Sobrido, L.; Krogan, N. J.; Ashworth, A.; Fraser, J. S.; Ott, M. A Single Inactivating Amino Acid Change in the SARS-CoV-2 NSP3Mac1 Domain Attenuates Viral Replication in Vivo. *PLoS Pathog.* **2023**, *19*, No. e1011614.

(6) Kerr, C. M.; Parthasarathy, S.; Schwarting, N.; O'Connor, J. J.; Pfannenstiel, J. J.; Giri, E.; More, S.; Orozco, R. C.; Fehr, A. R. PARP12 Is Required to Repress the Replication of a Mac1Mutant Coronavirus in a Cell- and Tissue-Specific Manner. *J. Virol.* **2023**, *97*, No. e0088523.

(7) Schuller, M.; Zarganes-Tzitzikas, T.; Bennett, J.; De Cesco, S.; Fearon, D.; von Delft, F.; Fedorov, O.; Brennan, P. E.; Ahel, I. Discovery and Development Strategies for SARS-CoV-2 NSP3Macrodomain Inhibitors. *Pathogens* **2023**, *12*, 324.

(8) Gahbauer, S.; Correy, G. J.; Schuller, M.; Ferla, M. P.; Doruk, Y. U.; Rachman, M.; Wu, T.; Diolaiti, M.; Wang, S.; Neitz, R. J.; Fearon, D.; Radchenko, D. S.; Moroz, Y. S.; Irwin, J. J.; Renslo, A. R.; Taylor, J. C.; Gestwicki, J. E.; von Delft, F.; Ashworth, A.; Ahel, I.; Shoichet, B. K.; Fraser, J. S. Iterative Computational Design and Crystallographic Screening Identifies Potent Inhibitors Targeting the Nsp3Macrodomain of SARS-CoV-2. *Proc. Natl. Acad. Sci. U. S. A.* **2023**, *120*, No. e2212931120.

(9) O'Connor, J. J.; Ferraris, D.; Fehr, A. R. An Update on the Current State of SARS-CoV-2 Mac1 Inhibitors. *Pathogens* **2023**, *12*, 1221.

(10) Wazir, S.; Parviainen, T. A. O.; Pfannenstiel, J. J.; Duong, M. T. H.; Cluff, D.; Sowa, S. T.; Galera-Prat, A.; Ferraris, D.; Maksimainen, M. M.; Fehr, A. R.; Heiskanen, J. P.; Lehtiö, L. Discovery of 2-Amide-3-Methylester Thiophenes That Target SARS-CoV-2 Mac1 and Repress Coronavirus Replication, Validating Mac1 as an Antiviral Target. *J. Med. Chem.* **2024**, *67*, 6519−6536.

(11) Pfannenstiel, J. J.; Duong, M. T. H.; Cluff, D.; Sherrill, L. M.; Colquhoun, I.; Cadoux, G.; Thorne, D.; Pääkkönen, J.; Schemmel, N. F.; O'Connor, J.; Saenjamsai, P.; Feng, M.; Parthasarathy, S.; Hageman, M. J.; Johnson, D. K.; Roy, A.; Lehtiö, L.; Ferraris, D. V.; Fehr, A. R. Identification of a Series of Pyrrolo-Pyrimidine-Based SARS-CoV-2 Mac1 Inhibitors That Repress Coronavirus Replication. *MBio* **2025**, *16*, No. e0386524.

(12) Suryawanshi, R. K.; Jaishankar, P.; Correy, G. J.; Rachman, M. M.; O'Leary, P. C.; Taha, T. Y.; Matsui, Y.; Zapatero-Belinchón, F. J.; McCavitt-Malvido, M.; Doruk, Y. U.; Stevens, M. G.; Diolaiti, M. E.; Jogalekar, M. P.; Chen, H.; Richards, A. L.; Kongpracha, P.; Bali, S.; Montano, M.; Rosecrans, J.; Matthay, M.; Togo, T.; Gonciarz, R. L.; Gopalkrishnan, S.; Neitz, R. J.; Krogan, N. J.; Swaney, D. L.; Shoichet, B. K.; Ott, M.; Renslo, A. R.; Ashworth, A.; Fraser, J. S. The Mac1 ADP-Ribosylhydrolase Is a Therapeutic Target for SARS-CoV-2. *eLife* **2025**, *14*, RP103484.

(13) Correy, G. J.; Rachman, M. M.; Togo, T.; Gahbauer, S.; Doruk, Y. U.; Stevens, M. G. V.; Jaishankar, P.; Kelley, B.; Goldman, B.; Schmidt, M.; Kramer, T.; Radchenko, D. S.; Moroz, Y. S.; Ashworth, A.; Riley, P.; Shoichet, B. K.; Renslo, A. R.; Walters, W. P.; Fraser, J. S. Exploration of Structure-Activity Relationships for the SARS-CoV-2 Macrodomain from Shape-Based Fragment Linking and Active Learning. *Sci. Adv.* **2025**, *11*, No. eads7187.

(14) Schuller, M.; Correy, G. J.; Gahbauer, S.; Fearon, D.; Wu, T.; Díaz, R. E.; Young, I. D.; Carvalho Martins, L.; Smith, D. H.; Schulze-Gahmen, U.; Owens, T. W.; Deshpande, I.; Merz, G. E.; Thwin, A. C.; Biel, J. T.; Peters, J. K.; Moritz, M.; Herrera, N.; Kratochvil, H. T.; QCRG Structural Biology Consortium; Aimon, A.; Bennett, J. M.; Brandao Neto, J.; Cohen, A. E.; Dias, A.; Douangamath, A.; Dunnett, L.; Fedorov, O.; Ferla, M. P.; Fuchs, M. R.; Gorrie-Stone, T. J.; Holton, J. M.; Johnson, M. G.; Krojer, T.; Meigs, G.; Powell, A. J.; Rack, J. G. M.; Rangel, V. L.; Russi, S.; Skyner, R. E.; Smith, C. A.; Soares, A. S.; Wierman, J. L.; Zhu, K.; O'Brien, P.; Jura, N.; Ashworth, A.; Irwin, J. J.; Thompson, M. C.; Gestwicki, J. E.; von Delft, F.; Shoichet, B. K.; Fraser, J. S.; Ahel, I. Fragment Binding to the Nsp3Macrodomain of SARS-CoV-2 Identified through Crystallographic Screening and Computational Docking. *Sci. Adv.* **2021**, *7*, No. eabf8711.

(15) Taha, T. Y.; Chen, I. P.; Hayashi, J. M.; Tabata, T.; Walcott, K.; Kimmerly, G. R.; Syed, A. M.; Ciling, A.; Suryawanshi, R. K.; Martin, H. S.; Bach, B. H.; Tsou, C.-L.; Montano, M.; Khalid, M. M.; Sreekumar, B. K.; Renuka Kumar, G.; Wyman, S.; Doudna, J. A.; Ott, M. Rapid Assembly of SARS-CoV-2 Genomes Reveals Attenuation of the Omicron BA.1 Variant through NSP6. *Nat. Commun.* **2023**, *14*, 2308.

(16) Collins, P. M.; Ng, J. T.; Talon, R.; Nekrosiute, K.; Krojer, T.; Douangamath, A.; Brandao-Neto, J.; Wright, N.; Pearce, N. M.; von Delft, F. Gentle, Fast and Effective Crystal Soaking by Acoustic Dispensing. *Acta Crystallogr. D Struct. Biol.* **2017**, *73*, 246−255.

(17) Kabsch, W. XDS. *Acta Crystallogr. D Biol. Crystallogr.* **2010**, *66*, 125−132.

(18) Evans, P. R.; Murshudov, G. N. How Good Are My Data and What Is the Resolution? *Acta Crystallogr. D Biol. Crystallogr.* **2013**, *69*, 1204−1214.

(19) Pearce, N. M.; Krojer, T.; Bradley, A. R.; Collins, P.; Nowak, R. P.; Talon, R.; Marsden, B. D.; Kelm, S.; Shi, J.; Deane, C. M.; von Delft, F. A Multi-Crystal Method for Extracting Obscured Crystallo-

https://doi.org/10.1021/acs.jmedchem.5c02933
J. Med. Chem. XXXX, XXX, XXX−XXX

graphic States from Conventionally Uninterpretable Electron Density. *Nat. Commun.* **2017**, *8*, No. 15123.
(20) Moriarty, N. W.; Grosse-Kunstleve, R. W.; Adams, P. D. Electronic Ligand Builder and Optimization Workbench (ELBOW): A Tool for Ligand Coordinate and Restraint Generation. *Acta Crystallogr. D Biol. Crystallogr.* **2009**, *65*, 1074−1080.
(21) Liebschner, D.; Afonine, P. V.; Baker, M. L.; Bunkóczi, G.; Chen, V. B.; Croll, T. I.; Hintze, B.; Hung, L. W.; Jain, S.; McCoy, A. J.; Moriarty, N. W.; Oeffner, R. D.; Poon, B. K.; Prisant, M. G.; Read, R. J.; Richardson, J. S.; Richardson, D. C.; Sammito, M. D.; Sobolev, O. V.; Stockwell, D. H.; Terwilliger, T. C.; Urzhumtsev, A. G.; Videau, L. L.; Williams, C. J.; Adams, P. D. Macromolecular Structure Determination Using X-Rays, Neutrons and Electrons: Recent Developments in Phenix. *Acta Crystallogr. D Struct. Biol.* **2019**, *75*, 861−877.
(22) Correy, G. J.; Kneller, D. W.; Phillips, G.; Pant, S.; Russi, S.; Cohen, A. E.; Meigs, G.; Holton, J. M.; Gahbauer, S.; Thompson, M. C.; Ashworth, A.; Coates, L.; Kovalevsky, A.; Meilleur, F.; Fraser, J. S. The Mechanisms of Catalysis and Ligand Binding for the SARS-CoV-2 NSP3Macrodomain from Neutron and x-Ray Diffraction at Room Temperature. *Sci. Adv.* **2022**, *8*, No. eabo5083.
(23) McCoy, A. J.; Grosse-Kunstleve, R. W.; Adams, P. D.; Winn, M. D.; Storoni, L. C.; Read, R. J. Phaser Crystallographic Software. *J. Appl. Crystallogr.* **2007**, *40*, 658−674.
(24) Emsley, P.; Lohkamp, B.; Scott, W. G.; Cowtan, K. Features and Development of *Coot*. *Acta Crystallogr. D Biol. Crystallogr.* **2010**, *66*, 486−501.
(25) Chai, J.-D.; Head-Gordon, M. Long-Range Corrected Hybrid Density Functionals with Damped Atom-Atom Dispersion Corrections. *Phys. Chem. Chem. Phys.* **2008**, *10*, 6615−6620.
(26) Weigend, F.; Ahlrichs, R. Balanced Basis Sets of Split Valence, Triple Zeta Valence and Quadruple Zeta Valence Quality for H to Rn: Design and Assessment of Accuracy. *Phys. Chem. Chem. Phys.* **2005**, *7*, 3297−3305.
(27) Marenich, A. V.; Cramer, C. J.; Truhlar, D. G. Universal Solvation Model Based on Solute Electron Density and on a Continuum Model of the Solvent Defined by the Bulk Dielectric Constant and Atomic Surface Tensions. *J. Phys. Chem. B* **2009**, *113*, 6378−6396.

https://doi.org/10.1021/acs.jmedchem.5c02933
J. Med. Chem. XXXX, XXX, XXX−XXX